Effectiveness of different advanced oxidation processes (AOPs) on the abatement of the model compound mepanipyrim in water

Article *in* Journal of Photochemistry and Photobiology A Chemistry · January 2016

DOI: 10.1016/j.jphotochem.2016.01.024

4 authors, including:

Filomena Lelario
Università degli Studi della Basilicata
45 PUBLICATIONS **198** CITATIONS
SEE PROFILE

Monica Brienza
Aristotle University of Thessaloniki
12 PUBLICATIONS **18** CITATIONS
SEE PROFILE

Sabino Aurelio Bufo
Università degli Studi della Basilicata
181 PUBLICATIONS **1,186** CITATIONS
SEE PROFILE

Journal of Photochemistry and Photobiology A: Chemistry 321 (2016) 187–201

Contents lists available at ScienceDirect

Journal of Photochemistry and Photobiology A: Chemistry

journal homepage: www.elsevier.com/locate/jphotochem

Effectiveness of different advanced oxidation processes (AOPs) on the abatement of the model compound mepanipyrim in water

F. Lelario[a,*], M. Brienza[a], S.A. Bufo[a], L. Scrano[b]

[a] Department of Sciences, University of Basilicata, Via dell'Ateneo Lucano 10, Potenza, Italy
[b] Department of European Cultures (DICEM), University of Basilicata, 85100 Potenza, Italy

ARTICLE INFO

Article history:
Received 13 March 2015
Received in revised form 18 January 2016
Accepted 23 January 2016
Available online 27 January 2016

Keywords:
Mepanipyrim
Ozone
Heterogeneous photocatalysis
Titanium dioxide
Pilkington Active™ Blue glass
Transformation products

ABSTRACT

This study aims to present the effectiveness of different advanced oxidation processes (AOPs) as photolysis (UV mercury arc and Xe-arc), ozone, ozone/Hg-UV, and photocatalysis (suspended and immobilized TiO_2) for the degradation of the fungicide mepanipyrim in aqueous solutions. A well-known commercial product Pilkington Active™ Blue glass has been tested as immobilized TiO_2 system. Experiments were performed in batch mode at laboratory scale and results were compared in terms of disappearance kinetics. Transformation products (TPs) were identified by Surveyor LC system coupled to a hybrid LTQ-FTICR (7-T) mass spectrometer (MS). Simple mechanisms of degradation for different AOPs were proposed. New by-products formed during the degradation processes were identified. Since primarily hydroxy derivatives were identified in aqueous suspensions, the mechanism of degradation was probably based on hydroxyl radical attack. The greatest difference in the quality of transformation products was observed between the heterogeneous photocatalysis using suspended TiO_2 and Pilkington Active™ Blue glass system. The inhibition percentage of bioluminescence from *Vibrio fischeri* – as a toxicity parameter – increased during the irradiation time due to the residual concentration of the parent compound and transformation products generated.

1. Introduction

Water purification is essential for human health, wildlife, and a balanced environment. In all the world, water is being polluted at unprecedented rates with chemicals, nutrients, metals, pesticides, and other contaminants. National Water-Quality Assessment (NWQA) investigation based on information from 51 of the Nation's most important river basins and aquifers in USA reports that 96% of all fish, 100% of all surface water samples and 33% of major aquifers contain one or more pesticides at detectable levels [1]. The widespread contamination of waterways with pesticides and their transformation products (TPs) is a serious threat to both public health and environmental integrity. The presence in the water of recalcitrant organic compounds like pesticides can be attributed to several sources, such as agriculture activity, industrial discharges [2], urban storm water runoff [3], and domestic uses of them.

The presence of low concentrations of resistant organic compounds and their TPs in the effluent from Waste Water Treatment Plants (WWTPs) has been detected, clearly showing that some of them cannot be eliminated during wastewater treatment [4,5]. For this reason, it is advisable to develop technologies as tertiary treatment processes, which could promote the easy degradation of recalcitrant compounds.

A promising way to perform the mineralization of these types of substances is the application of advanced oxidation processes (AOPs). The concept of "advanced oxidation processes" was established by Glaze et co-workers in 1987 [6]. AOPs were defined by the generation of hydroxyl radicals in aqueous solutions which achieve a great destruction power. The mostly investigated AOPs in wastewater treatment consist of UV, ozone and ozone/UV technologies. Processes based on ozone are extremely active, but a major disadvantage is that due to its instability, ozone must be generated before use and the equipment and operating costs can be quite high. Hence, other emerging technologies providing viable alternative are required.

TiO_2 catalyst exhibits very strong oxidation potential in presence of oxygen when irradiated by UV light or sunlight. Its relative oxidation power is almost twice higher than the oxidation power of ozone [7]. In fact, TiO_2, in anatase–rutile form, is used as a photocatalyst in the oxidation and removal of innumerable chemical pollutants in water and air [8,9]; as well as for disinfection of wastewater effluents [10–12].

* Corresponding author. Fax: +39 0 971206226.
E-mail address: filomenalelario@hotmail.com (F. Lelario).

http://dx.doi.org/10.1016/j.jphotochem.2016.01.024
1010-6030/

Photocatalytic processes on TiO_2 (TiO_2/UV) are based on generation of electron–hole pairs by the UV irradiation with energy in the range of the TiO_2 band gap, E_{bg} = 3–3.2 eV [13]. The active electron (−)–hole (+) pairs handles the redox reactions with various species adsorbed onto the semiconductor surface. The main advantages linked to the use of TiO_2 are the low toxicity and cost, commercial availability and chemical inertness. The weak points are: difficulty in filtering and recycling the photocatalyst, extinction of irradiation light due to scattering and absorption of the radiations by the particles themselves. To overcome these problems, research efforts have been spent for the immobilization of stable TiO_2 on supporting materials [14–18].

In this work, photolysis (by UV and simulated solar irradiation), ozone (coupled or not with UV), heterogeneous photocatalysis under simulated solar irradiation using two forms of TiO_2 (suspended or immobilized on the surface of thin glass plates) have been investigated to assess the suitability of different oxidation processes to promote mineralization of a recalcitrant pesticide. For this purpose, due to its wide use all over the world, and its accumulation in superficial and groundwater, mepanipyrim was chosen as a model compound representing an organic substance recalcitrant to many wastewater treatment processes [19].

Mepanipyrim is a fungicide adopted in agriculture against gray mold disease caused by *Botrytis cinerea* [20]. It is very persistent in water, wastewater, soil and food [21]. Krueger et al [22] reported the occurrence of mepanipyrim residues in water samples collected from six water courses, which were draining areas with horticultural crops in Sweden. Because of the widespread use of this chemical in the production of a very diffused food, people are exposed at different levels to the fungicide depending on their diets.

In most cases, the degradation rate or the organic compounds are calculated following the disappearance of the target substance as a function of time. However, due to the possibility of the formation of intermediate species, the total degradation of the target compound does not often corresponds to the total mineralization of the whole organic residues [23–25]. Therefore, it is important to investigate the mechanism of oxidation, identifying all the possible intermediate derivatives. Calza et al. [26] reported a study dealing with the degradation of mepanipyrim under heterogeneous photocatalysis by suspended TiO_2. This paper suggests a degradation pathway and proposes the formation of several intermediate compounds, but there is a lack of investigation on the degradation behaviour of mepanipyrim when other powerful oxidative processes are applied, and on the toxicant properties of degradation mixtures as compared to the parent compound.

Thus, the aim of this work was to test the efficiency of several induced abiotic degradation processes. The results of all processes were compared and the identification of transformation products was obtained by using a highly performed liquid chromatography–mass spectrometry technology. For identification, structural data were obtained with a hybrid quadrupole linear ion trap (LTQ) and Fourier-transform ion cyclotron resonance mass spectrometer (FTICR MS) following positive electrospray ionization (ESI). These data were complemented with accurate mass measurements on both precursor and fragment ions obtained using collision induced dissociation (CID) an Infrared Multiphoton Dissociation (IRMPD). Toxicity measurements of the treated solutions were carried out in order to evaluate the effectiveness of the treatment methods.

2. Experimental

2.1. Chemicals and materials

All chemicals were used of analytical grade. The standard active substance (AS) of mepanipyrim (*N*-(4-methyl-6-prop-1-inylpyrimidin-2-yl)anilin; elemental composition $C_{14}H_{13}N_3$; M.W. 223.27;

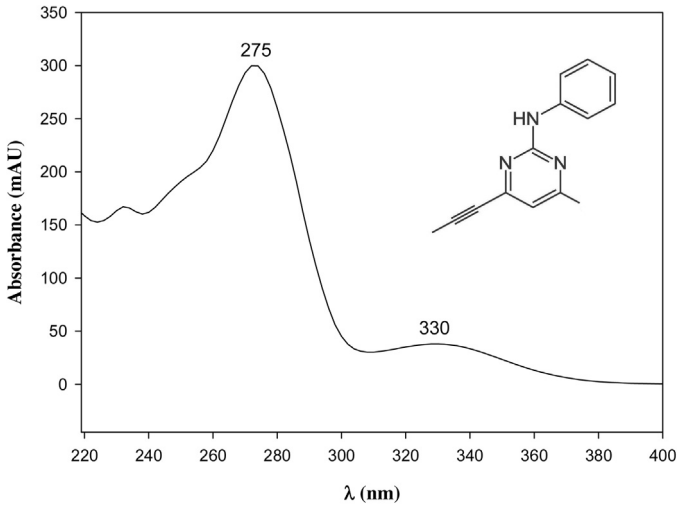

Fig. 1. Structure and UV absorption spectrum of mepanipyrim.

Fig. 1) was provided from Dr. Ehrenstorfer GmbH Augsburg, Germany, purity grade >99%. Uranyl oxalate (analytical grade) was purchased from Sigma-Aldrich (St. Louis, MO, USA); filters (disposable sterilized packet) were acquired from Fluka Chemie (Buchs, Switzerland). Ultrapure water was obtained by means of a Millipore (Billerica, MA, USA) Milli-Q system. LC/MS grade water, methanol and acetonitrile were from Carlo Erba (Milano, Italy). In the case of heterogeneous photocatalysis, two different forms of TiO_2 were used (i) Degussa P-25, obtained as a gift from Evonik (Hanau, Germany), primary particle size 20–30 nm by TEM and agglomerate-aggregate particle size 2.5–20 μm in wet environment, specific surface area of 54 $m^2 g^{-1}$ by BET, composition 78% anatase and 22% rutile by X-ray diffraction (technical information from manufacturer), UV absorption 280–400 nm wavelength; (ii) Pilkington Active™ Blue glass, kindly gifted from Pilkington glass (United Kingdom) as example of their commercially available product Active™ self-cleaning float glass. Float glass is a sheet of glass made by floating molten glass on a bed of molten metal. The float glass process is also known as the Pilkington process. The Active™ Blue glass has been obtained by a coating process using a nanocrystalline film of TiO_2 on 4 mm tin glass sheet. The catalyst has been deposited by means of an atmospheric pressure chemical vapour deposition technique (APCVD), as described in detail elsewhere [27].

2.2. Experimental devices for oxidation processes

Reactor A: All the oxidation experiments were done in 250 mL tubular oxidation reactor (Pyrex®) provided with a thermostatic jacket, and containing the fungicide aqueous solution. The temperature was maintained constant by circulating water from a thermostatic bath (25 ± 0.1 °C). The external reactor wall was covered with an aluminium foil as protection from external light. When the UV irradiation was required, a high pressure Hg lamp (HPK 125 W, Philips, Eindhoven, The Netherlands) was inserted in a quartz well placed at the middle of the reactor (Fig. 2A).

Reactor B: the photocatalytic experiments were carried out by using a cylindrical reactor (250 mL) covered with a quartz plate and placed in a solar simulator Atlas Suntest CPS+ (Atlas Material Testing Technology, Mount Prospect, IL, USA). The radiation source was a xenon lamp (1500 W, max power) placed in the upper part of the oven in the axis of a parabolic mirror (Fig. 2B). The temperature was kept constant (25 ± 0.1 °C) by means of an air conditioning system, and the solution was maintained under continuous stirring, which ensured an optimum mixing flow.

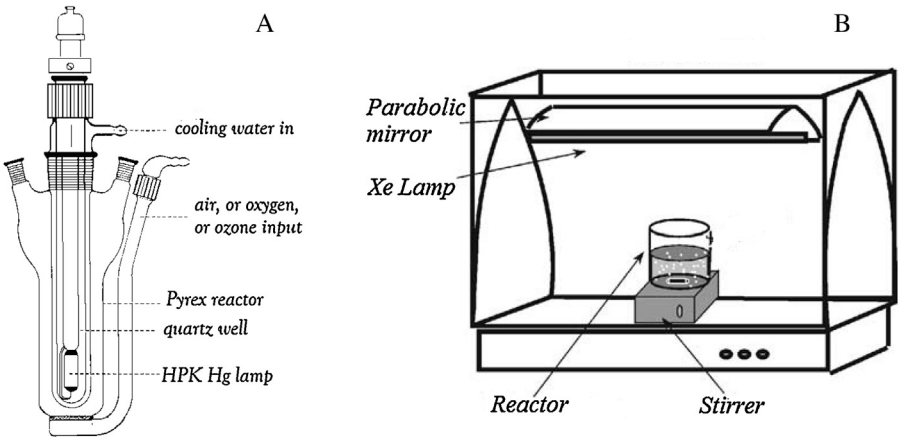

Fig. 2. Reactors utilized for photodegradation experiments: (A) high pressure Hg-UV lamp, HPK 125 W; (B) solar simulator "suntest".

All the experiments were performed at the initial concentration 22 mg L^{-1} of mepanipyrim. To avoid microbial contamination, all glass apparatus were heat sterilised by autoclaving for 60 min at 121 °C before use. Aseptic handling materials and laboratory facilities were used throughout the study to maintain sterility. Due to the low solubility of mepanipyrim in water [28] a stock solution (110 mg L^{-1}) of the pure standard AS in 5% methanol 95% ultrapure water was prepared and kept in the darkness at +4 °C. Calibration and test solutions were prepared when used by dilution of the stock solution. Three replicates were carried out for each experiment.

2.2.1. Photolysis

For treatments with artificial light sources, both the reactors A and B were used. (i) *Hg-UV irradiation*. With the Hg-UV lamp the total wavelength passing to the solution, taking in account the glass filtration, was in the range 290 nm $< \lambda <$ 580 nm, with centred wavelength at 365 nm. Actinometric measurements were performed by using uranyl oxalate photo-reaction to test the mercury arc efficiency at the beginning and the end of the experiment [29,30]. At the end of the irradiation experiment the efficiency of Hg-UV arc was not appreciably diminished from the reference value of 1.97×10^{16} photons cm^{-1} s^{-1}. (ii) *Xe-arc*. The xenon lamp supplies radiations in the range 300 nm $< \lambda <$ 800 nm, similar to those of sun. Before the beginning of the experimental work the light emission effectiveness of the irradiation system was tested by using the uranyl oxalate method [29,30]. The disappearance of oxalate was 7.2 10^{-4} mol s^{-1}. The mean integrated irradiance was 500 Wm^{-2} (in the full range 300–800 nm), and the radiant exposure for an irradiation time of 60 h was 108 MJ m^{-2} (300–800 nm). The surface of the cylindrical reactor offers an exposed area of 33.2 cm^2 permitting only irradiation of 1.66 W enters the samples. The measured irradiance was practically constant during the entire duration of the irradiation tests.

2.2.2. Ozone (O_3)

Ozonation was performed in the liquid phase by means of an ozone generator model OZ 500 MM from Fischer Technology (Bonn, Germany), using oxygen and dried air as feed gas. The equipment and experimental condition have been described elsewhere [31]. This equipment is able to produce a constant flow of O_3 obtained through an electrical discharge at high voltage. In our experiment we adjusted the oxygen/air enrichment at 60 L m^{-3} h^{-1} and the ozone production at 12 g m^{-3} h^{-1}. The ozone generator is furnished with a precision valve for the O_2 input and a needle valve for the O_3 output. Ozone was bubbled at a rate of 2 g h^{-1} through a Teflon® tube into the oxidation reactor (reactor A).

2.2.3. O_3/Hg-UV

The O_3/Hg-UV experiment was carried out following the same procedure used in the O_3 experiment but the Hg-UV lamp was put into the internal thimble of the reactor and turned on. The lamp was the same as that used for the photolysis experiment.

2.2.4. Photocatalysis

The heterogeneous photocatalysis experiment was carried out following the same procedure used for photolysis process under the xenon lamp irradiation in the solar simulator, but an amount of 0.2 g L^{-1} TiO_2, previously optimized as the more suitable ratio between the catalyst and the compound to be degraded, was added to the mepanipyrim solution. The mepanipyrim solution added with the appropriate amount of catalyst was magnetically stirred during the light irradiation. At specific time intervals, samples were collected from the reactor for analysis. In order to remove the TiO_2 powder the solution to be analysed was filtered through a 0.2 μm PTFE filter. For the experiments with immobilized TiO_2, the inner wall of the reactor was covered entirely with seven slabs of Pilkington Active™ Blue glass.

2.3. Analytical procedures

The identification of derivative compounds was performed by means of a LC–ESI–FTICR MS, liquid chromatography–mass spectrometry technology using electrospray ionization (ESI) coupled with a hybrid quadrupole linear ion trap (LTQ) and Fourier-transform ion cyclotron resonance mass spectrometer (FTICR MS) (Thermo Fisher Scientific, Bremen, Germany). LC separation were obtained by a Surveyor pump and Surveyor autosampler and a Discovery C_{18} column, 250 × 4.6-mm inner diameter, 5-μm particle size (pore size, 18 nm), equipped with a Discovery C_{18} 20 × 4-mm inner diameter security guard cartridge (Supelco Inc., Bellefonte, PA, USA), at ambient temperature. Sample volumes of 25 μL were injected. HPLC grade water (0.1% formic acid) was used as eluent A and acetonitrile as eluent B, in isocratic conditions at 45:55 ratio (A%:B%, v/v) for 15 min at a flow rate of 1.0 mL min^{-1}, which was split 4:1 after the analytical column to allow 200 μL min^{-1} to enter the ESI source. Positive ion ESI-MS was chosen for the detection of intermediate products of degradation in the range of m/z 50–800. The quantification of mother substance was obtained using an on-line diode array detector at 240 nm. The calibration curve exhibited linearity, and a determination coefficient (r^2) of 0.99997, in the range 0.22–22 mg L^{-1}. The limit of detection (LOD) of the used method was established to be 0.04 mg L^{-1}, on the basis of a pick area threefold higher than the

background noise, and the limit of quantification (LOQ) was set to 0.13 mg L^{-1} (3.3 × LOD).

2.4. Vibrio fischeri *bioassay*

The luminescence inhibition of marine bacteria *Vibrio fischeri* was evaluated using the Microtox® Toxicity Test. In the presence of pollutant agents the natural bioluminescence of *V. fischeri* is reduced and the toxicity end-point (EC_{50}) can be determined as the concentration of a tested sample that caused 50% reduction in light output. The acute bioluminescence assay was carried out according to ISO 113412-1,2,3 [32]. The luminescence inhibition of the extract was assessed carrying out the "81.9% Basic test protocol" (screening test) (Azur Environment Ltd., 1998) [33].

3. Results and discussion

3.1. Stability of mepanipyrim in aqueous solution

For the stability test, an aqueous solution (1% in MeOH) of 22 mg L^{-1} pure mepanipyrim, obtained by 5-fold water dilution of the stock solution, was kept in dark at room temperature for three days. Samples (1.5 mL) were taken during the experimental time and analysed. No degradation was noticed at the end of the experiment (72 h) resulting from possible thermal reactions. It is clearly concluded that mepanipyrim is stable in aqueous solution at room temperature.

3.2. Degradation of mepanipyrim by different AOPs

For all AOPs tested, kinetic parameters were calculated using integrated equations describing zero-, first-, and second-order reactions [34–38]:

$$C_t = C_0 - kt, \text{ zero} - \text{order} \quad (1)$$

$$C_t = C_0\, e^{kt}, \text{ first}-\text{order} \quad (2)$$

$$C_t = \frac{C_0\, t_{1/2}}{(t + t_{1/2})}, \text{ second}-\text{order} \quad (3)$$

where C_0 is the initial concentration of the reactant, C_t is the remaining concentration at time <t>, <k> is the kinetic constant, and $t_{1/2}$ is the half-life of the reactant.

According to Snedecor and Cochran [39]. the best fit was checked using the least square method of estimation.

The knowledge of reaction order is essential for finding the correct integrated rate equation and the implementation of a kinetic model for further applications. Adoption of above reported equations implies that photo-reactions are governed by simple kinetic laws, as

$$v = -\frac{dC_t}{dt} = k, \text{ zero} - \text{order} \quad (4)$$

$$v = -\frac{dC_t}{dt} = kC_t, \text{ first}-\text{order} \quad (5)$$

$$v = -\frac{dC_t}{dt} = kC_t^2, \text{ second}-\text{order} \quad (6)$$

where <v> is the reaction rate, <k> has been defined above.

Due to differences in the units to be attributed to their kinetic constants, reactions having different orders cannot be directly compared using these values (k). However, the efficiency of processes can be compared by the persistence of mepanipyrim under different treatments thanks to the observation of half-life values, which unit is always a time unit.

The significance of first- and second-order reactions has been well defined elsewhere [34–37,40], while, some definitions are due to explain the occurrence of a zero-order reaction. A zero-order occurs when the reaction rate is constant during the whole observation time (apparently it does not depend by the reactant concentration). This can happen when the concentration reduction per time unit is negligible with respect to the initial or remaining concentration. Zero-order kinetics is always an artefact of the conditions under which the reaction is carried out. For this reason, reactions that follow zero-order kinetics are often referred to as pseudo-zero-order reactions. A zero-order process cannot continue up to the reactant has been exhausted; before this point is reached, the reaction will revert to another rate law. There are two general conditions that can give rise to zero-order rates: (i) only a small fraction of the reactant molecules is in a location or state in which the substance is able to react, and this fraction is continually replenished from the larger pool; (ii) when two or more reactants are involved, the concentrations of some are much greater than those of others, this situation commonly occurs when a reaction is catalysed by attachment to a solid surface (heterogeneous catalysis) or to an enzyme [40].

3.2.1. Direct photodegradation

First photodegradation experiments were carried out employing either Hg-UV or Xe-arc light-irradiation of mepanipyrim to

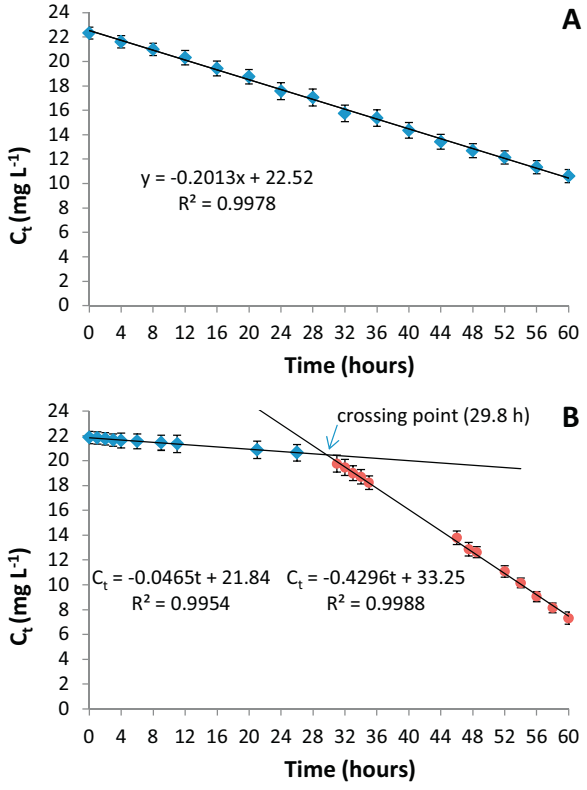

Fig. 3. Graphical estimation of mepanipyrim pseudozero-order kinetics of degradation reactions obtained in the Hg-UV (A) or Xe-arc (B) systems. Error bars represent the standard deviations calculated on three replicates.

determine direct photolysis. Fig. 3 shows the mepanipyrim degradation curves obtained with the Hg-UV (A) or Xe-arc (B) systems. In both cases slow degradation rates of the testing substance were found during the observation time. These results indicate that mepanipyrim is resistant to photolysis presumably due to its high chemical stability and relative low molar adsorption coefficient above 300 nm wavelength (Fig. 1)

Applying the least square method of estimation to Eqs. (1)–(3) for the assessment of kinetic parameters of the fungicide degradation reaction either under the Hg-UV- or Xe-arc- irradiation, the best fit was found in both cases when the linear Eq. (1), which describes pseudo zero-order reactions, was used (Fig. 3).

Consequently, the half-life was calculated rearranging Eq. (1) for $t = t_{1/2}$ and $C_t = 1/2\ C_0$:

$$t_{1/2} = \frac{C_0}{2k} \tag{7}$$

where $<C_0>$ is the concentration obtained from the intercept of curves shown in Fig. 3 at the initial time (zero), $<k>$ is the kinetic constant ($mg\,L^{-1}\,h^{-1}$) resulting from the slope of the curves.

Using the Hg-UV system, a half-life of 55.9 h was achieved under the experimental conditions realized. Due to the dependence of the half-life from the initial concentration found in the zero-order kinetics, it is clear that increasing or decreasing the $<C_0>$ amount, also the value of $<t_{1/2}>$ should vary correspondingly. Noteworthy, in the case of Xe-arc the system offers initially a strong inertia and only after 29.8 h of irradiation (crossing point in Fig. 3B), when at least 6.3% of initial AS concentration has been disappeared, the reaction rate increases to an acceptable value, giving a half-life of 38.7 h, and a degraded amount of 67% after 60 h-irradiation time.

The rationale behind of such a behaviour may be found considering that the total reaction rate during a photodegradation process in aqueous environments results by the sum of two or more reactions, which rates are normally different, being the formation of simple radicals the fastest and the formation of the active intermediate form (AIF) of the target substance the slowest [40]. The rate of final transformation into one or more photoproducts can be of the same magnitude order of the AIF formation or one or more orders higher [29,36,40]. That means that the rapidity with which the AIF reaches a concentration useful for the prosecution of the reaction can govern the whole process. Using Hg-UV system, the rate of disappearance of mepanipyrim is constant throughout the observation time (60 h), suggesting that (i) the formation of the active intermediate is the slower process governing the reaction; (ii) the useful concentration of AIF is reached in the first few minutes of reaction and remains constant during the whole experiment; (iii) the rate of AIF transformation into the final products is sufficiently high as not to affect the total speediness of the process. In the case of Xe-arc system, initially the process is slow and the apparent rate constant of the reaction ($0.0465\ mg\,L^{-1}\,h^{-1}$) is about one order of magnitude lower that the constant calculated for UV-Hg system ($0.2013\ mg\,L^{-1}\,h^{-1}$). At the crossing point (29.8 h) actually, the AIF reach a useful concentration for the final transformation into photoproducts with a different reaction rate, which is slowed down by the insufficient velocity of AIF formation.

3.2.2. Processes involving ozone

Also for the processes involving the use of ozone, the least square method of estimation was applied to Eqs. (1)–(3) for the assessment of kinetic parameters of the fungicide degradation reaction either under O_3 or O_3/Hg-UV-treatments. Both measured reaction rates were best fitted by the exponential Eq. (2) (Fig. 4A), which describe pseudo first-order reactions.

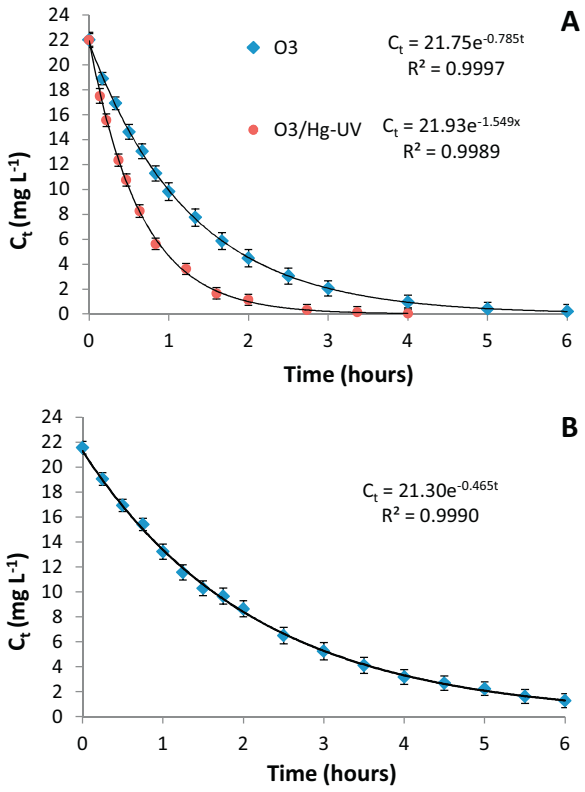

Fig. 4. Degradation curves and estimation of pseudo first-order kinetics for the reaction of mepanipyrim under O_3 or O_3/Hg-UV treatments (A), and in the TiO_2/Xe-arc photocatalytic system (B). TiO_2 concentration = $0.2\ g\,L^{-1}$. Error bars represent the standard deviations calculated on three replicates.

The half-life for pseudo first-order reaction was calculated using the linearized form of Eq. (2):

$$\mathrm{Ln}\,C_t = \mathrm{Ln}\,C_0 - kt \tag{8}$$

where $<C_0>$ is the concentration calculated at the initial time (zero), and $<C_t>$ is the remaining concentration of the studied substance at the time $<t>$.

Rearranging Eq. (8) for $t = t_{1/2}$ and $C_t = 1/2\ C_0$, it is easy to calculate the value of $t_{1/2}$ (Table 1):

$$t_{1/2} = \frac{\mathrm{Ln}2}{k} \tag{9}$$

where $<k>$ is the kinetic constant (h^{-1}) obtained from the slope of Eq. (8) relative to the curves reported in Fig. 4A.

Ozone treatment has proved very effective for removing mepanipyrim from the aqueous solution (Fig. 4A), reducing the initial concentration within the first 3 h of reaction of about 90%. The removal of mepanipyrim reached 99% in further 3 h. The first order rate constant (k) of mepanipyrim treated with O_3 was determined to be $0.785\ h^{-1}$ (Table 1). On the other hand, the reaction rate increased when O_3 was combined with Hg-UV irradiation ($k = 1.549\ h^{-1}$). The synergistic effect of O_3/Hg-UV is much more efficient in degrading mepanipyrim than the two separate processes, reaching 95% of fungicide degradation in two h.

Table 1
Determination coefficients of linearized kinetic equations (r^2), pseudo first-order kinetic constants (k) and half-lives ($t_{1/2}$) for the different AOPs.

Processes	r^2	k (h^{-1})	$t_{1/2}$ (h)
O_3	0.9997	0.785	0.88
O_3/Hg-UV	0.9989	1.549	0.45
Xe-arc/TiO_2	0.9990	0.465	1.5

After 4 h the concentration of the AS was below the limit of quantification.

3.2.3. Heterogeneous photocatalysis

A test experiment was carried out with suspended TiO_2 in the dark. This preliminary assay showed that mepanipyrim does not disappear in the dark in presence of TiO_2, ruling out the inexistence of any reaction such as hydrolysis or persistent adsorption. However, TiO_2 under Xe-arc irradiation significantly degraded the fungicide resulting in a typical photo-catalytic reaction.

Due to the inherent nature of a heterogeneous photocatalytic system using suspended TiO_2, it is necessary to find the optimum catalyst concentration at which the removal rate is at its maximum. In this study, the optimum was determined by changing the concentration of TiO_2 over the range 0–0.3 g L^{-1}. The addition of TiO_2 to the solution at a concentration of 0.1 g L^{-1} resulted in a rapid removal rate, which was further improved when the catalyst concentration was increased to 0.2 g L^{-1}. With additional increase of catalyst concentration to 0.3 g L^{-1} any improving or reduction of the removal rate was not observed; the added concentration was merely "passive" in photocatalytic terms (Fig. 5). The optimum catalyst concentration is a complex function of many parameters including catalyst agglomeration, the suspension opacity, light scattering, mixing, reactor type, and the pollutant type [41], and hence it cannot be equal for all photocatalytic systems [42]. In our case, no large agglomerations were visible also when 0.3 g L^{-1} of catalyst was added, but the suspension opacity augmented considerably suggesting the insurgence of significant scattering phenomena (not measured).

Also in the case of TiO_2/Xe-arc irradiation, the measured decreasing of the fungicide concentration was best fitted by the exponential Eq. (2) (Fig. 4B), which describe a pseudo first-order reaction.

Based on literature assessment of induced degradation reactions of organic pollutant in liquid phase, typically, they follow pseudo first order kinetics [31,37,43,44]. This was the case for O_3, O_3/Hg-UV and TiO_2/Xe-arc assays in our investigation. As a consequence, these different AOPs were compared according to the pseudo first order kinetics of mepanipyrim removal (Table 1).

$t_{1/2}$,

It should be considered that for first order kinetics the value of $t_{1/2}$ is independent from the concentration of the reactant; being $<k>$ a constant, $t_{1/2}$ assumes also a constant value. This observation is of concern from a technical point of view. We can speculate that when an oxidation process has to be chosen for a practical application as tertiary stage in tandem of a wastewater treatment plant, it is easier to manage a system which effectiveness is independent from the initial concentration of pollutants to be removed than a process that needs continuously adjustments in function of the contaminant concentrations in the secondary effluent.

The TiO_2/Xe-arc system was able to reduce the initial concentration of mepanipyrim of about 74% within the first 3 h of reaction, and of 94% in 6 h (Fig. 4B). The first order rate constant (k) was calculated to be 0.465 h^{-1}. The effectiveness of the fungicide degradation using the three AOPs reported in Table 1 was compared considering the half-life values of the respective reactions, which were (in the order of increasing efficiency) TiO_2/Xe-arc (1.5 h or 90 min), O_3 (0.88 h or 53 min), O_3/Hg-UV (0.45 h or 27 min).

3.2.4. Photocatalysis using immobilized TiO_2 in the Xe-arc system

By using SEM image of the cross section sample of the Pilkington Active™ Blue glass (Fig. 6), the thickness of TiO_2 film was found to be 397 nm. EDX analysis (Table 2) of the glass surface coated with TiO_2, compared to the composition of the glass core showed that TiO_2 is a component present only on the glass surface along with other metal oxides such as iron oxide. As reported in the Pilkington patent, cobalt oxide is present in low amounts (less than 75 μg/g) and is not detectable by EDX analysis. Cobalt oxide may confer the blue colour to the glass.

For the experiments with immobilized TiO_2, seven slabs of Pilkington Active™ Blue glass (7.5 × 2.0 × 0.4 cm, Fig. S1) were necessary to cover entirely the inner wall of the reactor B (Fig. 2).

The reaction rate of the fungicide degradation in this system was best fitted by linear equations (Fig. 7), which describe zero-order reactions. As in the case of Xe-arc (Fig. 3B), the Xe-arc/Pilkington Active™ Blue glass system offers a relative inertia in the first part of the process, and only after 11.9 h of irradiation (crossing point in Fig. 7), when at least 8.4% of initial concentration has been degraded, the reaction rate increases to an acceptable value, giving a halflife of 23.4 h, and a degraded amount of 95% after 45 h-irradiation time.

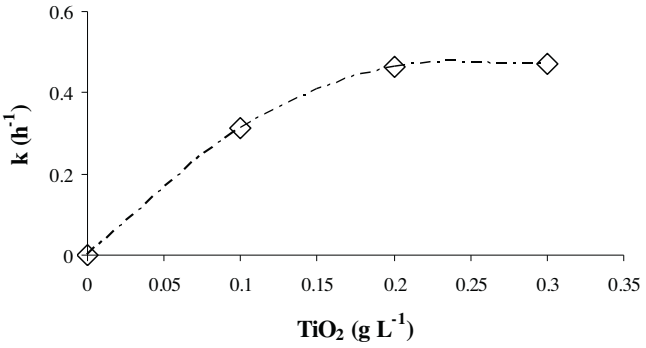

Fig. 5. Rate constant variation vs. TiO_2 suspended amount for the photocatalysis of mepanipyrim degradation in the Xe-arc system.

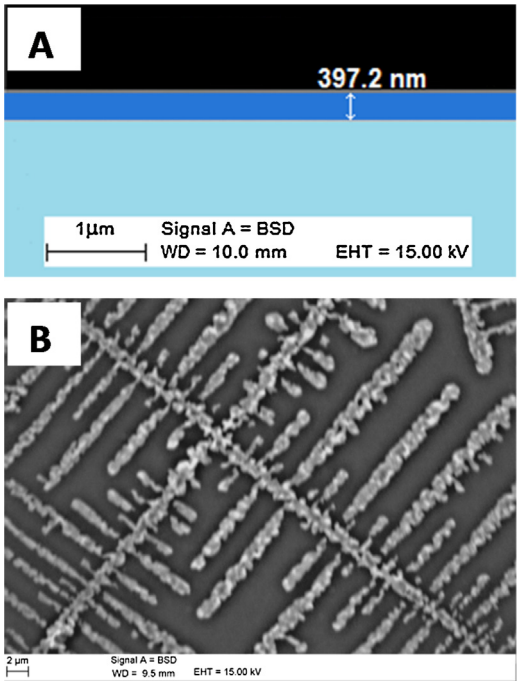

Fig. 6. (A) SEM reconstructed and colored micrograph of the Pilkington Active™ Blue glass cross section showing the TiO_2 layer immobilized on the glass surface; (B) SEM original micrograph of the Blue glass surface showing the fine-toothcomb of TiO_2 coating.

Table 2
EDX analysis of the glass surface coated with TiO_2(Pilkington Active™) compared to the glass core composition.

Elemental composition of the grafted surface Energy: 6.686 KeV, counts: 250		Elemental composition of the core glass Energy: 6.686 KeV, counts: 250	
Elements	Wt.% ± SD	Elements	Wt.% ± SD
O	44.4 ± 0.4	O	47.2 ± 0.4
Si	38.6 ± 0.2	Si	36.2 ± 0.2
Na	6.0 ± 0.2	Na	4.3 ± 0.1
Ca	5.5 ± 0.2	Ca	6.0 ± 0.1
Mg	2.4 ± 0.1	Mg	2.4 ± 0.1
Ti	1.5 ± 0.1	Sn	2.1 ± 0.1
K	0.3 ± 0.05	K	0.3 ± 0.05
Al	0.3 ± 0.05	Al	1.0 ± 0.05
Fe	0.3 ± 0.05	Fe	0.4 ± 0.1
		Cl	0.1 ± 0.05

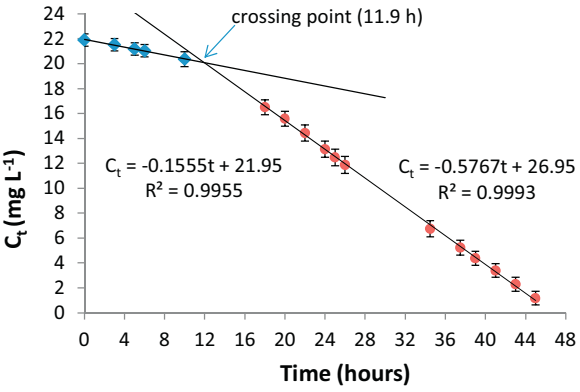

Fig. 7. Graphical estimation of mepanipyrim pseudo zero-order kinetics of the degradation reaction obtained in the TiO_2 immobilized system (Pilkington Active™ Blue glass). Error bars represent the standard deviations calculated on three replicates.

The kinetic constant was 0.1555 mg L^{-1} h^{-1} in the first part of the reaction and increased to 0.5767 mg L^{-1} h^{-1} after the crossing point time.

Main goals chased in this case were the comparison of two catalysis methods by the observation of degradation profiles as well as the reaction kinetics and transformation products. Comparing the two heterogeneous processes experimented, the lowest degradation efficiency was obtained using Pilkington Active™ Blue glass and the highest with TiO_2 in suspension; giving 7% and 94% of mepanipyrim disappearance after 6 h of treatment, respectively. But, the photoreaction with Xe-arc irradiation in the presence of Blue glass was faster than the reaction under simple Xe-arc irradiation, testifying that the thin layer of the catalyst immobilized on the glass surface is able to accelerate the photodegradation of the fungicide.

The process exhibiting the lowest value of the half-life is O_3/Hg-UV, 124 and 86 times lower than both direct photodegradation methods, Hg-UV and Xe-arc, respectively, 52 times lower than Xe-arc/Pilkington Active™ Blue, 3.3 times lower than photocatalysis process using suspended TiO_2 and about two times lower than ozonation.

Although the photodegradation with the Xe-arc/Pilkington Active™ Blue system may implicate the production of hydroxyl radicals to achieve the removal of mepanipyrim as the suspension of TiO_2 powder does, the former is different from the last since it works with a very low useful concentration of the catalyst. Mepanipyrim has to interact closely with the surface of the glass covered with a very thin layer of TiO_2 in order to the reaction can occur, and it is mostly probable that the reaction products desorbs slowly to the solution. This can explain the greater time required to

Table 3
Major intermediate compounds formed during photodegradation processes identified as intact protonated molecules, $[M+H]^+$, by high resolution LC-ESI-FTICR MS.

N°	Intermediate compounds			Photodegradation process					
	Accurate *m/z* ratio as $[M+H]^+$	Molecular formula	Error (ppm)	Hg-UV	O_3	O_3/Hg-UV	Xe-arc	TiO_2/Xe-arc	Xe-arc/ P. Active Blue
1	240.11324	$C_{14}H_{13}N_3O$	0.4	X	X	X	X	X	X
2	240.11322	$C_{14}H_{13}N_3O$	0.3	X	X	X	X	X	X
3	240.11325	$C_{14}H_{13}N_3O$	0.5	X	X	X	X	X	X
4	240.11330	$C_{14}H_{13}N_3O$	0.7	X	X	X	X	X	X
5	254.09256	$C_{14}H_{11}N_3O_2$	0.6	X		X		X	
6	256.10828	$C_{14}H_{13}N_3O_2$	0.9	X		X		X	
7	256.10791	$C_{14}H_{13}N_3O_2$	−0.5	X		X		X	
8	256.10812	$C_{14}H_{13}N_3O_2$	0.3	X		X		X	
9	256.10822	$C_{14}H_{13}N_3O_2$	0.6	X		X		X	
10	148.08690	$C_8H_9N_3$	−0.2	X		X	X	X	X
11	238.09764	$C_{14}H_{11}N_3O$	0.6			X		X	
12	202.09758	$C_{11}H_{11}N_3O$	0.4	X	X	X	X	X	X
13	202.09755	$C_{11}H_{11}N_3O$	0.3	X	X	X	X	X	X
14	242.12891	$C_{14}H_{15}N_3O$	0.5	X	X	X	X	X	X
15	244.14464	$C_{14}H_{17}N_3O$	0.8	X	X			X	
16	260.13956	$C_{14}H_{17}N_3O_2$	0.8	X	X			X	
17	260.13953	$C_{14}H_{17}N_3O_2$	0.7	X	X			X	
18	258.12370	$C_{14}H_{15}N_3O_2$	−0.2		X			X	
19	274.11856	$C_{14}H_{15}N_3O_3$	−0.2			X	X	X	X
20	274.11856	$C_{14}H_{15}N_3O_3$	−0.4			X	X	X	X
21	244.10822	$C_{13}H_{14}N_3O_2$	0.7			X	X	X	X

degrade the fungicide under this processes. From this observations, the Pilkington Active™ Blue glass could be considered not useful, but by a practical point of view, it can constitute a promising material for the elimination of recalcitrant compounds from wastewater avoiding the removal of the catalyst after the photodegradation process. Probably, a further improvement of the effectiveness of Blue glasses could be obtained by modifying the nature and concentration of metal oxides used in the formulation of the glass. The ideal system, as stated above, should be governed by first-order kinetics rather than the zero-order reaction.

3.3. Intermediate transformation products (TPs)

In this study, mepanipyrim has been degraded using different processes and the feasible intermediates arising from the reactions were detected and tentatively identified by LC–FTICR MS. More than 21 compounds could be detected as possible degradation intermediates. The presence of these TPs was evaluated through an accurate analysis of extracted ion chromatograms (XICs) generated post acquisition from the total ion chromatogram (TIC) with a tight mass-to-charge window of ±0.0010 units around each selected ion of interest (Table 3). Fig. 8 shows the TIC and the accurate mass XICs of a sample of mepanipyrim solution after 3 h of photodegradation in presence of TiO_2 powder under Xe-arc irradiation (solar simulator), with the peak number used to identify each intermediates and the range of monoisotopic value as $[M+H]^+$ ion (m/z). The parent molecule of mepanipyrim elutes about at 6.5 min and exhibits an accurate m/z ratio of 224.11847 ($C_{14}H_{14}N_3$error 1.1 ppm). The product ion mass spectra of mepanipyrim was examined to obtain useful information for the interpretation of the product ion spectra of the unknown degradation products, so the positive ion electrospray CID and IRMPD MS/MS spectra of mepanipyrim are shown in Fig. 9A and B respectively. In the CID spectrum the two most abundant fragment ions were detected at m/z 209 and 183, due to the loss of CH_3 and CH_3CN radicals, and the accurate masses of these ions in the IRMPD spectrum were consistent with elemental compositions of $C_{13}H_{11}N_3^+$ and $C_{12}H_{11}N_2^+$, respectively. The ions of nominal m/z 207 and 131 corresponded to the structures with elemental composition $C_{14}H_{11}N_2^+$ and $C_8H_7N_2^+$, due to the neutral loss of ammonia (NH_3) and aniline (C_6H_7N), respectively. In addition, in the IRMPD spectrum the concomitant loss of ammonia and hydrogen radical ($^\bullet H$) yields to the formation of ion of m/z 206.08409 corresponding to elemental composition of $C_{14}H_{10}N_2^+$. The most prominent signal in the IRMPD spectrum is the $C_6H_5^+$ ion whit an accurate m/z value of 77.03864, corresponding to the phenyl ion. Several other fragment were found and many of the dominant fragment ions formed were the same from both the technique, CID and IRMPD. The elemental composition and the corresponding error in ppm for all fragments detected as protonated ions are reported in Fig. 9B and are in agree with the structures of the main fragments reported in a previous study [26].

All TPs observed in Fig. 8(C–K) show shorter retention times than the initial compounds, in accordance with their higher polarities. Amongst these, at this time of degradation the most abundant intermediates were the compound at exact m/z 242.12879 and the four species at exact m/z 240.11330, corresponding to different isomers obtained by non selective hydroxylation of the mepanipyrim on different position: the nitrogen bridge between the two rings, the phenyl ring, the heteroatomic ring and the propynilic chain [19,26]. In order to study the fragmentation of TPs in detail, spectra of each compound as $[M+H]^+$ were measured by CID and IRMPD MS/MS. Table 4 shows data related to the experimental masses of the protonated ion fragments, the error in ppm and the proposed empirical formula corresponding to the fragments identified. The resulting accurate

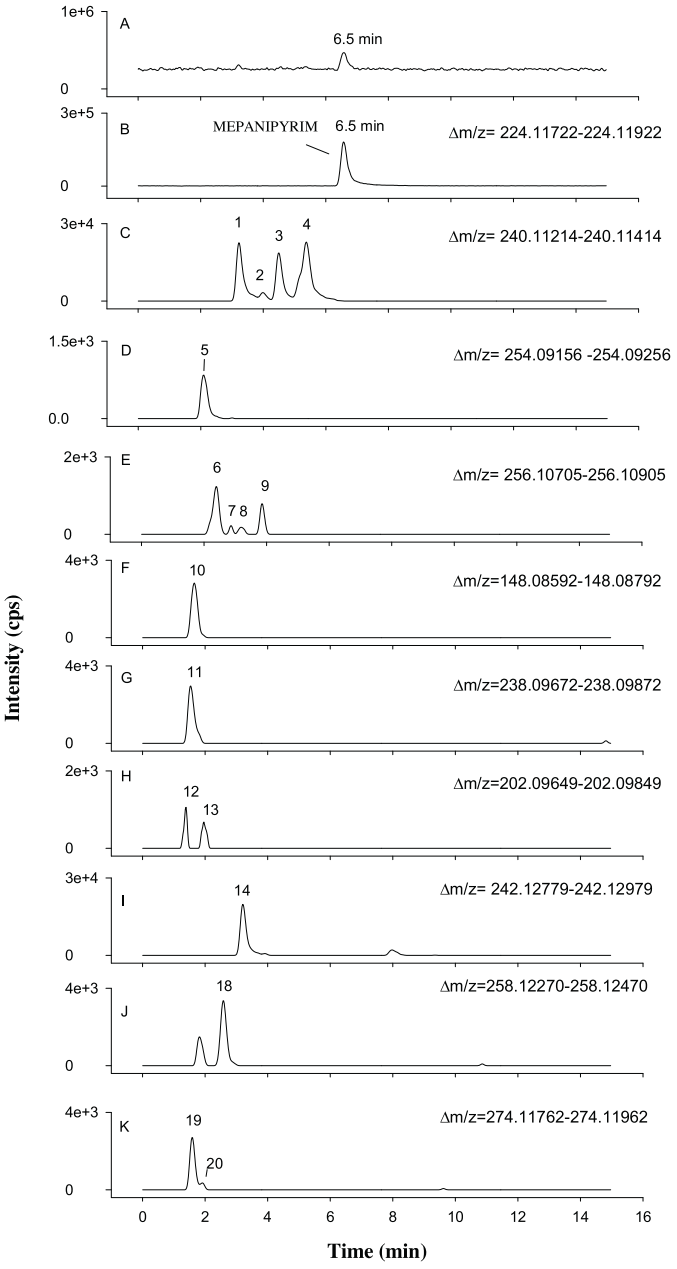

Fig. 8. Extracted ion chromatograms (XICs) using high resolution LC-ESI-FTICR MS acquired in positive ion mode mepanipyrim solution after three hours of photodegradation in presence of TiO_2 powder. The ions monitored correspond to the most abundant protonated molecules, $[M+H]^+$, using a restricted window of ±0.0010 m/z unit centred around each selected ion.

masses for these ions were found at an error less than 2.0 ppm in all cases.

Based on accurate mass measurement, fragment peaks observed and literature data [19,26], to four peaks at exact m/z 240.11330 were assigned the structure labelled 1–4 in Fig. 10. The precise assignment of these isomers is not possible, but differences observed in their mass spectra allow us to propose some structural differences as shown in Fig. 10.

Structural information enabling the identification of the —OH position in the compounds 1–4 is mainly provided by the mass peaks at m/z 225.09001, 199.08687 and 147.07932 (Table 4), corresponding to a CH_3 radical loss from the propynilic chain, a release of a CH_3CN following the cleavage of C—N and C—C bonds and an aniline neutral loss, respectively. The formation of these

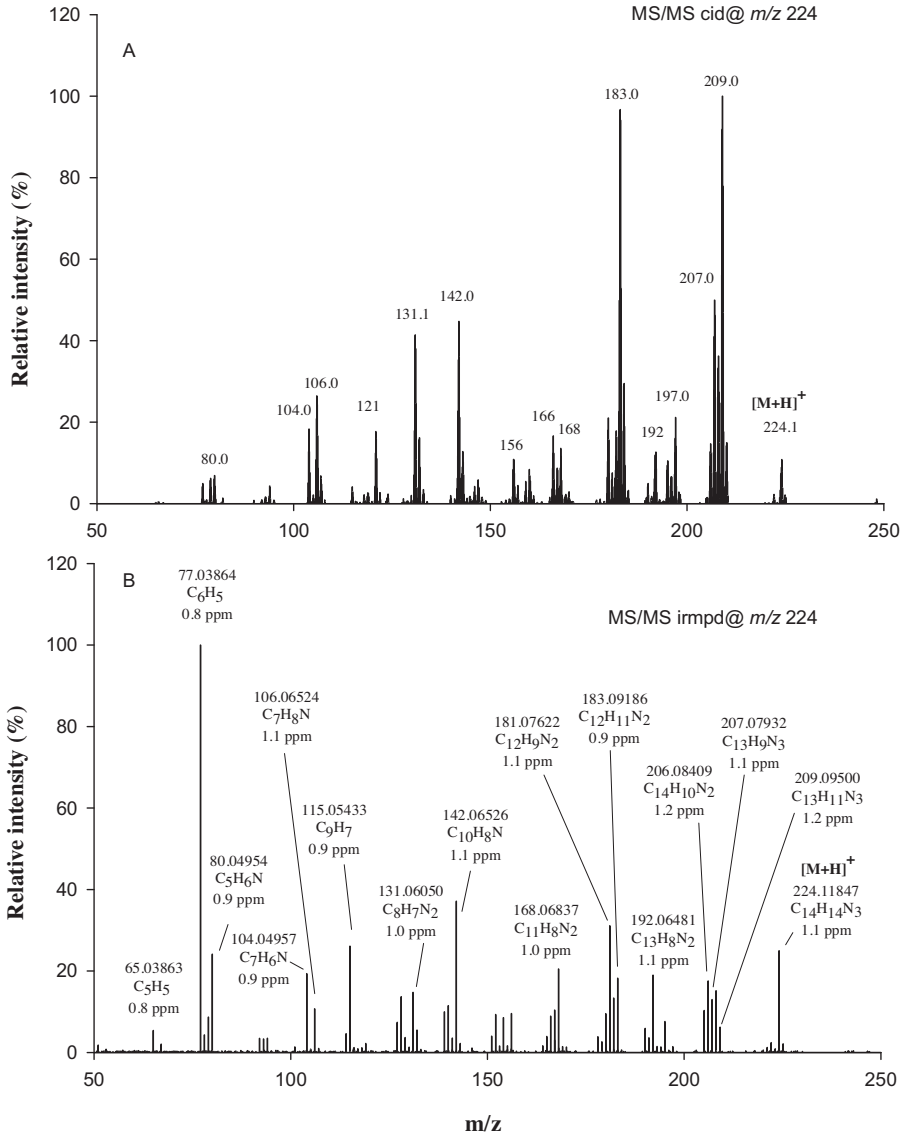

Fig. 9. CID (A) and IRMPD FTICR (B) MS/MS product ion spectra of the protonated mepanipyrim at *m*/*z* 224.

three fragments ions at *m*/*z* 225.09001, 199.08687 and 147.07932 corresponding to peaks detected at nominal *m*/*z* 209, 183 and 131 in the mass spectrum of mepanipyrim (Fig. 9), permits to exclude, for the compounds 1 and 3, the occurrence of OH group on the propynilic chain and heteroatomic ring. Moreover, the formation of a intense fragments at *m*/*z* 131.06055 and 223.08687 $[M+H-17]^+$, the last corresponding to the loss of OH group, in the tandem mass spectrum of compound 1, is compatible with a hydroxylation of the nitrogen bridge between the two rings [45]. Accordingly, the hypothesis was made that compound 3 is formed by a monohydroxylation of the phenyl ring. (Fig. 10). Although available structural information does not allow the precise position of the •OH radical attack to be predicted, considerations concerning the reactivity of the different sites on the mepanipyrim molecule suggests hydroxylation at position 4, which is para to an NH substituent on the aromatic ring and would be the most reactive toward oxidants. In the CID and IRMPD MS/MS spectra of compound 2, the occurrence of fragment ions at accurate *m*/*z* 225.09003 ($C_{13}H_{11}ON_3^+$, 1.6 ppm), due to the CH_3 radical loss from propenylic chain, and 147.05539 (C_8H_7 ON_2^+, 0.7 ppm), corresponding to neutral loss of aniline, together with the absence of CH_3CN loss (*m*/*z* 199) is indicative that the —OH group is, in this case, bonded to the pyrimidine ring, in position 4. This position is highly favourable for electrophilic attack because of the higher electron density of the pyrimidine ring. We wish to mention that the high mass resolving power of FTICR MS allow to distingue the fragments with the same nominal *m*/*z*, i.e. 147, found in tha mass spectra of all four isomers, that for compounds 1 and 3 (fragment 147.07932, $C_8H_9N_3^+$) confirm the monohydroxylation of the phenyl ring or the nitrogen bridge between the two rings, while for compounds 2 and 4 (fragment 147.05543, $C_8H_7ON_2^+$) exclude the monohydroxylation in these positions. The compound 10 showed an accurate mass of *m*/*z* 148.08692, which fits the formula $C_8H_9N_3$ (neutral molecule, −0.2 ppm error), corresponding to the loss of phenol group from the compound 3, trought the photodegradative process.

Compounds 5–9, exhibited an accurate *m*/*z* at 256.10805 with a difference of 32 amu respect to *m*/*z* ratio of protonated mepanipyrim molecule without variation from mepanipyrim in the degree of unsaturation suggesting the formation of dihydroxyl derivatives obtained by electrophilic substitution of two hydrogen atoms of mepanipyrim by hydroxyl radicals. The comparison of low and high relolution MS/MS spectra of all four compounds found at nominal *m*/*z* 256 did not provide information to assign

Table 4
CID and IRMPD FTICR MS product ions obtained from the protonated ions of the major intermediate compounds formed during photodegradation processes.

Compound (n)[a]	Precursor ion[b]	Main CID MS/MS product ions	Main IRMPD MS/MS product ions (accurate m/z)[c] and mass error (ppm)[d]
1	240	225, 223, 212, 199, 197, 181, 106,	225.09001 ($C_{13}H_{11}ON_3^+$, 1.5 ppm), 223.08687 ($C_{14}H_{11}ON_2^+$, 0.8 ppm), 212.11839 ($C_{13}H_{12}ON_2^+$, 0.8 ppm), 199.08687 ($C_{12}H_{11}ON_2^+$, 1.4 ppm), 197.09491 ($C_{12}H_{11}N_3^+$, 0.8 ppm), 181.07626 ($C_{12}H_9N_2^+$, 0.6 ppm), 147.07932 ($C_8H_9N_3^+$, 1.5 ppm), 131.06055 ($C_8H_7N_2^+$, 1.3 ppm), 106.06532 ($C_7H_8N^+$, 1.8 ppm), 94.06529 ($C_6H_8N^+$, 1.7 ppm), 92.049635 ($C_6H_6N^+$, 1.6 ppm), 80.04960 ($C_5H_6N^+$, 1.5 ppm),
2	240	225, 221, 212, 207, 197,181, 147, 121, 104, 94	225.09003 ($C_{13}H_{11}ON_3^+$, 1.6 ppm), 221.09497 ($C_{14}H_{11}N_3^+$, 1.0 ppm), 212.11845 ($C_{13}H_{12}ON_2^+$, 1.1 ppm), 207.07927 ($C_{13}H_8N_2^+$, 0.8 ppm), 197.09494 ($C_{12}H_{11}N_3^+$, 0.9 ppm), 181.07614 ($C_{12}H_9N_2^+$, 0.6 ppm), 147.05539 ($C_8H_7ON_2^+$, 0.7 ppm), 121.07612 ($C_{12}H_9N_2^+$, 0.8 ppm), 104.04955 ($C_7H_6N^+$, 0.7 ppm), 94.06520 ($C_6H_8N^+$, 0.8 ppm)
3	240	225, 223, 212, 199, 197, 147, 106, 94	225.09002 ($C_{13}H_{11}ON_3^+$, 1.6 ppm), 223.08701 ($C_{14}H_{11}ON_2^+$, 1.8 ppm), 212.11852 ($C_{13}H_{14}N_3^+$, 1.4 ppm), 199.08696 ($C_{12}H_{11}ON_2^+$, 1.8 ppm), 197.09488 ($C_{12}H_{11}N_3^+$, 0.7 ppm), 147.07935 ($C_8H_9N_3^+$, 1.6 ppm), 131.06052 ($C_8H_7N_2^+$, 1.1 ppm), 106.06528 ($C_7H_8N^+$, 1.4 ppm), 121.07621 ($C_7H_9N_2^+$, 1.5 ppm), 94.06525 ($C_6H_8N^+$, 1.4 ppm)
4	240	223, 212, 199, 197, 147, 122, 104, 94	223.08675 ($C_{14}H_{11}ON_2^+$, 0.7 ppm), 221.07166 ($C_{14}H_9ON_2^+$, 1.0 ppm), 207.07930 ($C_{13}H_9N_3^+$, 0.7 ppm), 199.08679 ($C_{12}H_{11}ON_2^+$, 1.0 ppm), 197.09488 ($C_{12}H_{11}N_3^+$, 0.7 ppm), 192.06833 ($C_{12}H_{11}ON_2^+$, 0.6 ppm), 147.05543 ($C_8H_7ON_2^+$, 1.0 ppm), 122.06017 ($C_7H_8ON^+$, 1.0 ppm) 104.04955 ($C_7H_6N^+$, 0.7 ppm), 94.06520 ($C_6H_8N^+$, 0.8 ppm)
5	254	236, 226, 212, 194	236.08202 ($C_{14}H_{10}ON_3^+$, 0.8 ppm), 226.08177 ($C_{13}H_{12}ON_3^+$, 1.2 ppm), 224.09775 ($C_{13}H_{10}ON_3^+$, −0.3 ppm),
6	256	239, 238, 228, 147, 135, 133, 92	238.09772 ($C_{14}H_{12}ON_3^+$, 1.0 ppm), 228.11327 ($C_{13}H_{14}ON_3^+$, 0.6 ppm), 226.09769 ($C_{13}H_{12}ON_3^+$, 1.0 ppm), 212.08209 ($C_{12}H_{10}ON_3^+$, 1.1 ppm), 198.06636 ($C_{11}H_8ON_3^+$, 0.9 ppm), 169.07617 ($C_{11}H_9N_2^+$, 0.9 ppm), 159.05544 ($C_9H_7ON_2^+$, 0.9 ppm), 147.05540 ($C_8H_7ON_2^+$, 0.7 ppm), 143.06050 ($C_9H_7N_2^+$, 0.9 ppm), 135.05539 ($C_7H_7ON_2^+$, 0.7 ppm), 133.07611 ($C_7H_7N_3^+$, 0.9 ppm), 131.06047 ($C_8H_7N_2^+$, 0.7 ppm), 94.06520 ($C_6H_8N^+$, 0.9 ppm), 92.04955 ($C_6H_6N^+$, 0.9 ppm), 80.04954 ($C_5H_6N^+$, 0.7 ppm),
7	256	238, 228, 226, 215, 210, 200, 198, 181	238.09772 ($C_{14}H_{12}ON_3^+$, 1.0 ppm), 210.10268 ($C_{13}H_{13}N_3^+$, 0.5 ppm), 200.11858 ($C_{12}H_{14}N_3^+$, 1.8 ppm), 198.06636 ($C_{11}H_8ON_3^+$, 0.9 ppm), 181.07610 ($C_{12}H_9N_2^+$, 0.4 ppm), 168.06830 ($C_{11}H_8N_2^+$, 0.6 ppm), 143.06050 ($C_9H_7N_2^+$, 0.9 ppm), 133.07611 ($C_8H_9N_2^+$, 0.90 ppm), 131.06047 ($C_8H_7N_2^+$, 0.7 ppm), 92.04955 ($C_6H_6N^+$, 0.90 ppm), 80.04954 ($C_5H_6N^+$, 0.7 ppm),
8	256	238, 228, 226, 215, 211, 210, 199	238.09767 ($C_{14}H_{12}ON_3^+$, 0.8 ppm), 210.10268 ($C_{13}H_{12}N_3^+$, 0.5 ppm), 169.07603 ($C_{11}H_9N_2^+$, 0.03 ppm), 92.04954 ($C_6H_6N^+$, 0.7 ppm), 80.04952 ($C_5H_6N^+$, 0.6 ppm),
9	256	239, 228, 215, 211, 197,187, 163, 159, 147, 135, 133, 94	238.09767 ($C_{14}H_{12}ON_3^+$, 0.8 ppm), 211.08670 ($C_{13}H_{11}ON_2^+$, 0.8 ppm), 197.07109 ($C_{12}H_9ON_2^+$, 0.7 ppm), 187.08682 ($C_{11}H_{11}ON_2^+$, 0.7 ppm), 169.07617 ($C_{11}H_9N_2^+$, 0.9 ppm), 159.05537 ($C_9H_7ON_2^+$, 0.5 ppm), 147.05539 ($C_8H_7ON_2^+$, 0.7 ppm), 135.05539 ($C_7H_7ON_2^+$, 0.7 ppm), 133.07613 ($C_8H_9N_2^+$, 0.9 ppm), 119.06046 ($C_7H_7N_2^+$, 0.7 ppm) 94.06519 ($C_6H_8N^+$, 0.7 ppm), 92.04955 ($C_6H_6N^+$, 0.90 ppm), 81.03355 ($C_5H_5O^+$, 0.6 ppm), 77.03863 ($C_6H_5^+$, 0.7 ppm)
10	148	131, 121, 106, 104, 80	133.06351 ($C_7H_7N_3^+$, 0.9 ppm), 131.06046 ($C_8H_7N_2^+$, 0.7 ppm), 106.06519 ($C_7H_8N^+$, 0.6 ppm), 104.04955 ($C_7H_6N^+$, 0.7 ppm), 80.04952 ($C_5H_6N^+$, 0.6 ppm), 77.03863 ($C_6H_5^+$, 0.7 ppm)
11	238	223, 221, 210, 197, 181	221.09493 ($C_{14}H_{11}N_3^+$, 0.8 ppm), 210.10276 ($C_{13}H_{12}N_3^+$, 0.9 ppm),
12	202	185, 160, 118, 84	185.07108 ($C_{11}H_9ON_2^+$, 0.7 ppm), 160.07581 ($C_{10}H_{10}ON^+$, 0.7 ppm), 132.08088 ($C_9H_{10}N^+$, 0.9 ppm) 118.07112 ($C_8H_8N^+$, 0.7 ppm), 84.04445 ($C_4H_6ON^+$, 0.7 ppm)
13	202	185, 160, 118, 84	185.07108 ($C_{11}H_9ON_2^+$, 0.7 ppm), 160.07581 ($C_9H_{10}N^+$, 0.7 ppm), 84.04445 ($C_4H_6ON^+$, 0.7 ppm)
14	242	224, 214, 200	224.11832 ($C_{14}H_{14}N_3^+$, 0.4 ppm), 207.07921 ($C_{13}H_9N_3^+$, 0.5 ppm), 200.11844 ($C_{12}H_{14}N_3^+$, 1.0 ppm), 195.09171 ($C_{13}H_{11}N_2^+$, 0.2 ppm), 131.06044 ($C_8H_7N_2^+$, 0.5 ppm), 104.04954 ($C_7H_6N^+$, 0.6 ppm), 77.03862 ($C_6H_5^+$, 0.6 ppm)
15	244	226, 216, 200, 125, 108	226.13409 ($C_{14}H_{16}N_3^+$, 1.0 ppm), 210.10272 ($C_{13}H_{12}N_3^+$, 0.7 ppm), 200.11842 ($C_{12}H_{14}N_3^+$, 0.9 ppm), 197.09477 ($C_{12}H_{11}N_3^+$, 0.1 ppm), 167.07306 ($C_{12}H_9N^+$, 0.6 ppm), 133.07611 ($C_8H_9N_2^+$, 0.6 ppm), 125.10746 ($C_7H_{10}N^+$, 0.6 ppm), 118.08088 ($C_7H_{13}N_2^+$, 1.0 ppm) 108.08084 ($C_7H_{10}N^+$, 0.6 ppm), 106.06520 ($C_7H_8N^+$, 0.7 ppm), 93.05736 ($C_6H_7N^+$, 0.6 ppm), 80.04952 ($C_5H_6N^+$, 0.5 ppm)
16	260	242, 230, 218	242.12881 ($C_{14}H_{16}ON_3^+$, 0.1 ppm), 224.11848 ($C_{14}H_{13}N_3^+$, 1.2 ppm), 218.09253 ($C_{11}H_{12}O_2N_3^+$, 0.6 ppm), 199.08678 ($C_{12}H_{11}ON_2^+$, 0.5 ppm), 108.08083 ($C_7H_{10}N^+$, 0.5 ppm), 93.05734 ($C_6H_7N^+$, 0.4 ppm), 80.04951 ($C_5H_6N^+$, 0.4 ppm)
17	260	242, 230, 225, 214, 108	242.12883 ($C_{14}H_{16}ON_3^+$, 0.2 ppm), 225.10236 ($C_{14}H_{13}ON_2^+$, 0.5 ppm), 214.13402 ($C_{13}H_{16}N_3^+$, 0.7 ppm), 184.07578 ($C_{12}H_{10}ON^+$, 0.5 ppm), 108.08083 ($C_7H_{10}N^+$, 0.5 ppm), 93.05734 ($C_6H_7N^+$, 0.4 ppm), 80.04951 ($C_5H_6N^+$, 0.4 ppm)
18	258	240, 228, 216, 198	240.11325 ($C_{14}H_{14}ON_3^+$, 0.5 ppm), 216.11327 ($C_{12}H_{14}ON_3^+$, 0.6 ppm), 198.10269 ($C_{12}H_{12}N_3^+$, 0.6 ppm), 186.10269 ($C_{11}H_{12}N_3^+$, 0.6 ppm), 171.09175 ($C_{11}H_{11}N_2^+$, 0.4 ppm)
19	274	256, 238, 228, 214	256.10812 ($C_{14}H_{14}O_2N_3^+$, 0.3 ppm), 238.09773 ($C_{14}H_{12}ON_3^+$, 1.0 ppm), 228.11325 ($C_{14}H_{12}ON_3^+$, 0.5 ppm), 220.08714 ($C_{14}H_{10}N_3^+$, 1.0 ppm), 214.09775 ($C_{12}H_{12}ON_3^+$, 1.2 ppm)
20	274	256, 228,	256.10848 ($C_{14}H_{14}O_2N_3^+$, 1.7 ppm), 228.11333 ($C_{14}H_{12}ON_3^+$, 0.8 ppm), 171.09183 ($C_{11}H_{11}N_2^+$, 0.9 ppm)
21	244	226, 202, 185,	202.09763 ($C_{11}H_{12}ON_3^+$, 0.7 ppm) 185.07109 ($C_{11}H_9ON_2^+$, 0.8 ppm), 160.07581 ($C_9H_{10}N^+$, 0.7 ppm), 84.04443 ($C_4H_6ON^+$, 0.5 ppm)

[a] n is the number used to identify each intermediate compounds in the chromatograms of Figs. 8 and 10.
[b] Isolated precursor ion for IRMPD fragmentation of protonated intermediate molecules.
[c] Significant signals with signal-to-noise ratio 5 or higher were taken into consideration.
[d] Mass error in part per million (ppm) evaluated as $10^6 \times$ (experimental accurate mass − monoisotopic calculated mass)/monoisotopic calculated mass.

unequivocally the position OH groups, but linking together the retention times with fragmentations of the individual peaks compared to those of monohydroxylated compounds, and taking into account data reported in literature [19,26,45,46], at the specific individual intermediates 6–9 are tentatively assigned the structures reported in Fig. 10. On the basis of the same considerations made for the compounds 1–4, compounds 6 and 7 could be obtained by a second hydroxylation of compound 1 in two different position. A confirmation on the occurrence of one OH group on the pyrimidine ring in the compound 6 can be obtained by identifying the ions at m/z 228.11327 ($C_{13}H_{14}ON_3^+$, 0.6 ppm) and at m/z 131.06047 ($C_8H_7N_2^+$, 0.7 ppm) resulting from the loss of CO from parent protonated molecule and from a fragment at accurate m/z 159.05544 ($C_9H_7ON_2^+$, 0.9 ppm), respectively. Still further

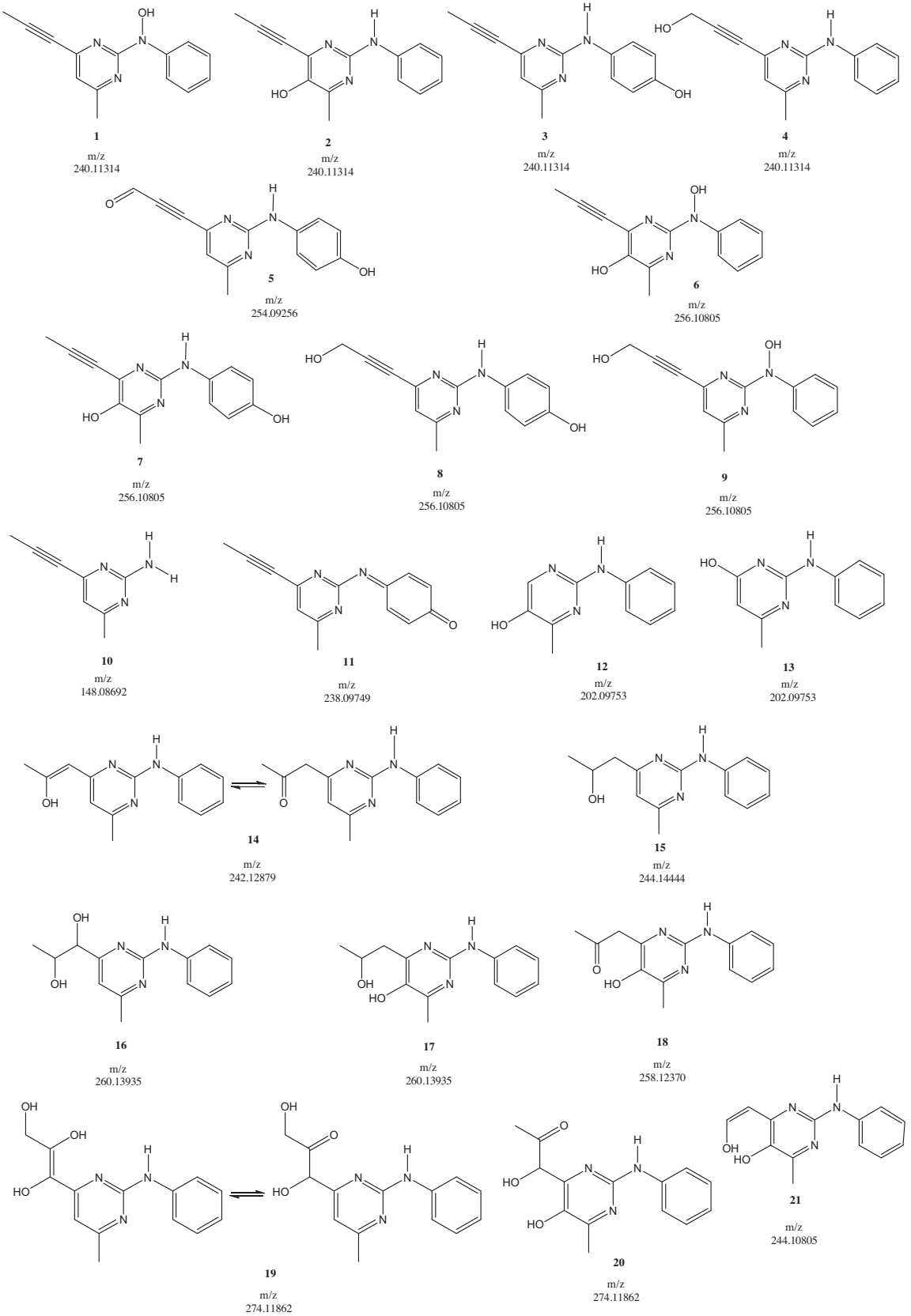

Fig. 10. Proposed structures major intermediates products generated by most photodegradation processes identified by LC–FTICR MS system and corresponding exact *m*/*z* ratios as $[M+H]^+$.

confirmation on the nature of structure 6 can be obtained by the occurrence of ion at *m*/*z* 239 in CID spectrum of this compound, that in accordance with the considerations made for compound 1 corresponds to a loss of a −OH group by the nitrogen bridge between the two rings. Similar to compound 1 the mass spectrum of compound 9 shows a fragmentation ion at $[M+H-17]^+$ corresponding to loss of OH bonded to the N-atom in the amine group of mepanipyrim. The other OH group is probably on the propynilic chain, as suggested by the occurrence of fragment ions at 147.05539 ($C_8H_7ON_2^+$, 0.7 ppm) and 135.05539 ($C_7H_7ON_2^+$, 0.7 ppm) in IRMPD spectrum, indicating the monohydroxylation of the propynilic chain or of the heteroatomic ring, and fragment ion at *m*/*z* 215 $[M+H—CH_3CN]^+$ in the CID spectrum of this compound. According to consideration made for compound 1, the CH_3CN loss (*m*/*z*) is indicative that the OH group is not bonded to the pyrimidine ring, so we can conclude that in this case the —OH group is on the propynilic chain. Taking into account the occurrence of a dominant fragment ion at *m*/*z* 228 in CID spectrum and the formation of fragment ion at *m*/*z* 200.11858 ($C_{12}H_{14}N_3^+$, 0.7 ppm) in the IRMPD spectrum, corresponding to the loss of one and two CO group respectively, we suggest for compound 7 a structure with one hydroxyl group on the pyrimidine ring and one on the phenyl ring; while the formation of fragment ions at *m*/*z* 211 $[M+H—CO—NH_3]^+$ and 199 in the low resolution MS/MS spectrum of compound 8, suggests for this compounds a structure with one hydroxyl group on the propynilic chain and one on the phenyl ring.

The compound 5 found at exact *m*/*z* 254.09256, is probably formed by a oxidation of compound 8 on the propynilic chain, as suggested by the presence of fragment peak at *m*/*z* 226.08177 $[M+H\text{-}CO]^+$ and *m*/*z* 212 $[M+H—CH_2=C=O]^+$. In the mass spectra of compound 11 at *m*/*z* 238.09764, the presence of the fragmentation peak at $[M+H-15]^+$ corresponding to a loss of radical CH_3, absent in the previous case, and peak at $[M+H-28]^+$ confirm that the initial degradation of mepanipyrim was due to attack by •OH radicals on the aromatic ring, yielding a mono-hydroxylated derivative, which is further oxidized into the corresponding quinone imine intermediate. to benzene ring in para position.

The two isomers at exact *m*/*z* 202.09753 were tentatively assigned, in order of elution, as structures 12 and 13 (Fig. 10). These two species presented mass spectra which were very similar, with loss compatible with the proposed structures (Fig. 11): the formation of the fragment at *m*/*z* 185.07108 ($C_{11}H_9ON_2^+$,

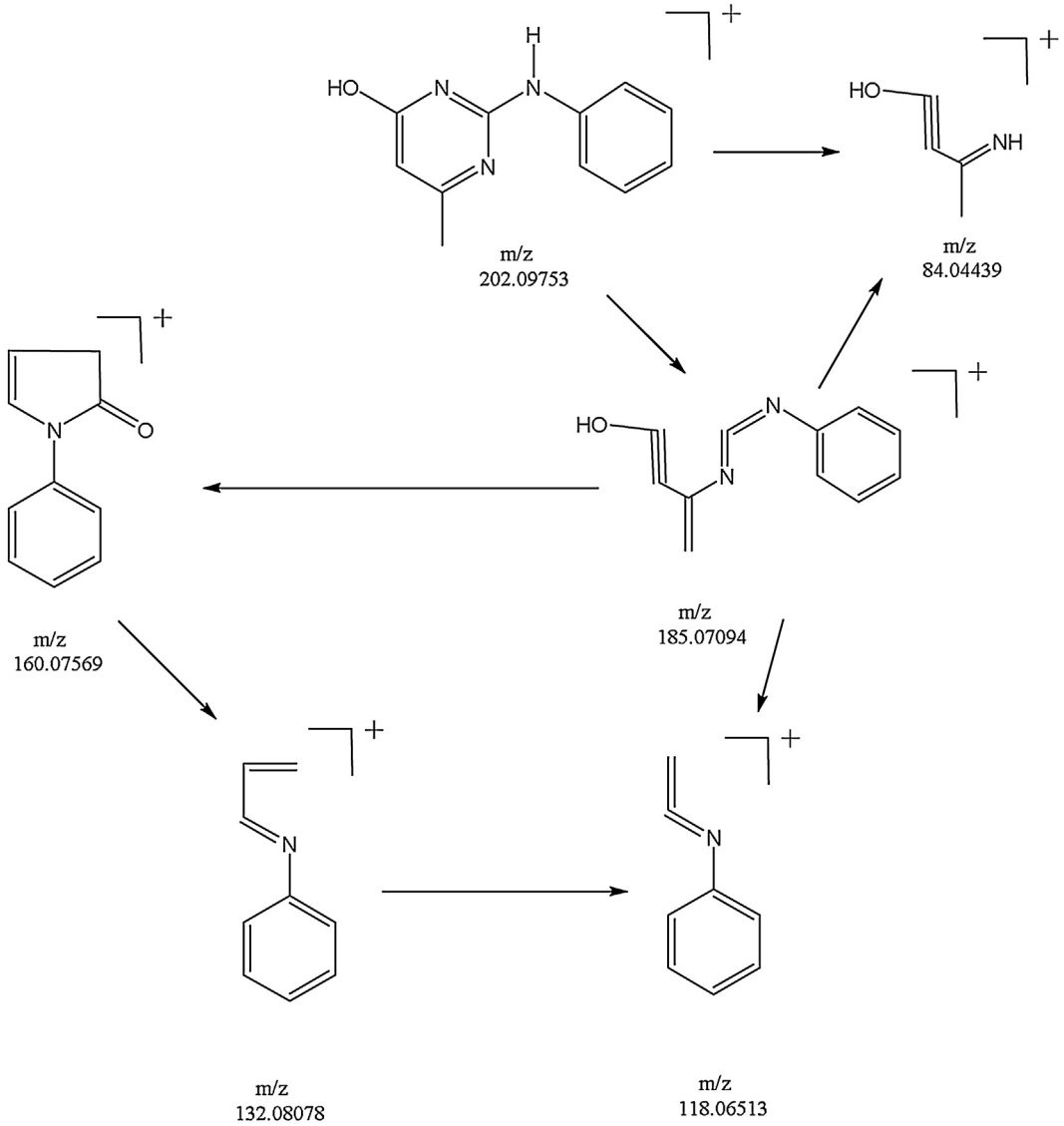

Fig. 11. Fragmentation pathways proposed for intermediate 12 (*m*/*z* 202.09753).

0.7 ppm), in the mass spectrum of compounds 12, is due to the neutral loss of NH_3, the fragment ion at *m/z* 132.08088 ($C_9H_{10}N^+$, 0.9 ppm). can be attributed to a structure coming from the fragment ion at *m/z* 160.07581 through the loss of —CO, and the formation of ion at *m/z* 84.04445 ($C_4H_6ON^+$, 0.7 ppm) implies that an OH group is located in the pyrimidinic moiety.

Structure identification of TPs allowed the assessment of the main degradation routes of mepanipyrim. In all of the photodegradation processes the formation of initial intermediates involves the attack by hydroxyl group on different positions of mepanipyrim structure, leading to the initial formation of the four isomeric forms of the compound at exact *m/z* 240.11314 and molecular formula $C_{14}H_{13}N_3O$, and subsequently to the formation the possible major intermediates reported in Fig. 10, according to the mechanisms proposed in Fig. S2 [26]. The reaction pathways proposed, although with some similarities, differ from others previously reported in the literature.

For all the processes of photodegradation it is also possible an initial formation of compounds at exact *m/z* 242.12879 and 244.1444 with molecular formula $C_{14}H_{15}N_3O$ and $C_{14}H_{17}N_3O$, respectively, through the attack of the •OH radical and the reduction of the triple bond, as suggested from variation of the insaturation degree with respect to mepanipyrim.

These intermediates can be subjected to other attack by •OH radical leading to the formation of two isomers at exact *m/z* 260.13935, and subsequently to the formation of other two isomers at exact *m/z* 274.11862, according to the mechanisms proposed in Fig. S3 [26].

The structures of these degradation product were confirmed by the appearance of the characteristic fragment in low and high resolution MS/MS spectra. The complete informations obtained from the CID and IRMPD fragments of these TPS were summarized in Table 4 with their molecular formula and the measured mass accuracies in ppm. As mentioned above, the compound at *m/z* 242.12879 has been initially seen in great amount (Fig. 8) and could be formed through the oxidation of the alcoholic group into an aldehydic one. This structure is in equilibrium with its tautomeric form as suggested by the presence of fragment peak at *m/z* 224.11832 $[M+H—CO]^+$, 200.11844 $[M+H\text{-}CH_2{=}C{=}O]^+$ and *m/z* 214 $[M+H-18]^+$, the last due to the loss of water from enolic form. Similary, the structure proposed for the degradation product at *m/z* 244.14444 was confirmed by the appearance of analogue fragments at *m/z* 226.13409 $[M+H—CO]^+$, *m/z* 216 $[M+H-18]^+$ and 200.11842 $[M+H—CH_3—CH{=}O]^+$. For this compounds we found fragment different with respect to those proposed in literature [26]. Actually, we detected an other compound with nominal *m/z* 244 but accurate *m/z* 244.10822, which fits the formula $C_{13}H_{14}N_3O_2$ (neutral molecule, 0.7 ppm error), tentatively assigned to the structure proposed in Fig. 10 (compound 21). Data obtained from MS/MS spectra confirmed the structure proposed, showing the formation of same fragments already discussed for compounds 12 and the occurrence of the ion fragment at *m/z* 202.09763 $[M+H—CH_2{=}C{=}O]^+$ obtained by a loss of ketene from parent molecule. To further confirm of the structure proposed, the unsaturation degree of this compound (RDB 8.5) resulted higher with respect to compound 15 (7.5), lower with respect to mepanipyrim (RDB 9.5) and the same of the compound 14 (RDB 8.5).

Two peaks at nominal *m/z* 260 correspondent to diidroxy derivatives (see compounds 16 and 17 in Fig. 10) and two peaks at nominal *m/z* 274 correspondent to triidroxy derivatives are also observed (see compounds 19 and 20 in Fig. 10). The predominant peaks in the MS/MS spectra of compound 16 are at *m/z* 242.12881 $[M+H-18]^+$ and *m/z* 224.11848 $[M+H-18-18]^+$, corresponding to a loss of one or two molecules of water, respectively, and the peak at *m/z* 218.09253 $[M+H—CH_2{=}C{=}O]^+$which is a good clue of a structure with two —OH on the propyl side chain. As above mentioned, the presence of a product ion at *m/z* 199.08678, in which the CH_3CN group is lost, may be seen as a further demonstration of the absence of the OH group on the pyrimidine ring in position 4. Instead, the presence of the last fragment was not observed in MS/MS spectra of compound 17, suggesting that, in this case, one —OH group is bonded to the pyrimidine ring; while the other OH group is probably bond to propyl chain, as showed from the presence of fragment ion at *m/z* 242.12883 $[M+H-18]^+$. The base peak at *m/z* 214.13402 $[M+H—18—CO]^+$ arising from the concomitant neutral losses of water and CO group was observed to occur in both low and high relotution MS/MS spectra. This product ion is of particular significance as it allows to confirm the position of OH groups in the structure proposed.

A peak at *m/z* 258.12370, correspondent to the keto-derivative of compound 17, is also observed in the solution at this time of degradation (compound 18, Fig. 8J). The occurrence of fragment ion at 240.11325 $[M+H\text{-}18]^+$, and 198.10269 $[M+H—18—CH_2{=}C{=}O]^+$ suggests that the oxidation occurs on the propanolic chain.

Based on the accurate mass of the protonated molecules, for isomer compounds 19 and 20 at exact *m/z* 274.11862 (Fig. 8, K) the $C_{14}H_{15}N_3O_3$ formula (RDB 8.5) was proposed with a low error (less than −0.4 ppm). leading to plausible structures consistent with the addition of three OH radical and electrons to mepanipyrim structure. Since there was a decrease of a unit in the RDB with the addition of three OH groups, the occurrence of only a double bond in the side chain was expected.

For compound 19 the loss of one and two water molecules, peaks at *m/z* 256.10812 ($C_{14}H_{14}O_2N_3^+$, 0.3 ppm) and 238.09773 ($C_{14}H_{12}ON_3^+$, 1.0 ppm), respectively, and the occurrence of peaks at *m/z* 238.09773 $[M+H—18—CO]^+$ arising from the concomitant neutral losses of water and CO group and *m/z* 214.09775 were indicative of the location of three OH groups in the propynylic chain. Unlike, the interpretation of the accurate mass and empirical formula of the fragment ions for compound 20 was consistent with a structure in which two OH groups are located in the propynylic chain and one in the pyrimidine ring. In particular, the presence of peak at *m/z* 171.09183 $[M+H—CH_3CHO—HCNO_2]^+$ is of particular significance as it allows to confirm the position of one OH group in the pyrimidine ring [26].

In the same way major photoproducts were detected and identified by LC–FTICR MS for all the processes under investigation. Table 3 summarizes the results of photoproducts' analyses in the different photodegradation processes (Hg-UV, O_3, O_3/Hg-UV, Xe-arc, TiO_2/Xe-arc, Xe-arc/P. Active Blue), highlighting the major intermediates identified amongst those shown in Fig. 8 for each photodegradation process, their monoisotopic exact value as protonated ions $[M+H]^+$ (*m/z*), the molecular composition and the mass error. It is worth noting, that in Xe-arc and Xe-arc/P. Active Blue glass photodegradation processes not only some of the possible intermediates reported in Fig. 8 were detected, but also conjugation molecules with accurate *m/z* ratio at 443.19803 (error 0.35 ppm), 443.19827 (error 0.56 ppm) and 461.20859 (error 0.64 ppm). The formation of conjugation molecules in these processes can be due to the presence of high amounts of molecules of mepanipyrim in solution for a time longer than the other AOPs experimented (O_3, O_3/Hg-UV, TiO_2/Xe-arc). The monoisotopic exact value as protonated ions $[M+H]^+$ (*m/z*), the molecular composition and the mass error of these compounds are reported in Table 5. The elucidation of the structure needs further investigations.

Some other minor peaks in the TIC chromatogram were identified as possible TPs, but no reliable assignation of their structures could be attained.

The complete degradation of mepanipyrim and its TPs was obtained only in the case of the three powerful AOPs adopted

Table 5
Proposed transformation products generated only by photolysis and Pilkington Active™ Blue glass identified, as intact protonated molecules, $[M+H]^+$, by high resolution LC-ESI-FTICR MS.

No.[a]	Accurate m/z[c] $[M+H]^+$	Molecular formula	Tr[b] (min)	Error[d] (ppm)
22	443.19803	$C_{28}H_{23}N_6$	3.1	0.35
23	443.19827		3.4	0.56
24	461.20859	$C_{28}H_{25}ON_6$	1.25	0.06

[a] No. is the number used to identify each compound.
[b] Retention times of compounds eluted under the experimental conditions described in the materials and method section.
[c] Accurate mass value of protonated molecules.
[d] Mass error in part per million, ppm = $10^6 \times$ (accurate mass − exact mass)/exact mass.

(O_3, O_3/Hg-UV, TiO_2/Xe-arc), as no peaks were observed in the mass chromatogram of the sample collected at the end of the experimental time utilized.

3.4. Toxicity of mepanipyrim and its transformation products

In order to evaluate the suitability of the photocatalytic treatment and to complement the information about the hazardousness of a treated effluent to the environment, the bioluminescence inhibition assay using *V. fischeri* was adopted.

Fig. 12 depicts the toxicity evolution of O_3/Hg-UV products using *V. fischeri* bioassay. This performance was selected amongst all the other degradation methods tested because it was considered the more representative due to the presence of the major number of transformation products (Table 3) in the samples collected in the range of 0–180 min. The toxicity of transient organic compounds, that may be more toxic than the mother molecules, was monitored in order to provide a more realistic scenario for the detoxification process under investigation, even if all TPs are completely disappeared at the end of the selected process.

The data of potential toxicity of treated mepanipyrim solution were described using a system of toxicity classification proposed by Persoone et al. [47]. The results of toxicity test were examined by calculating the Toxicity Unit (TU) as the inverse of EC_{50} value obtained for samples collected at different degradation times:

$$TU = \frac{100}{EC_{50}}$$

The untreated solution gave 2.22 TU and after 60 min of treatment the TU decreased up to 1.72, but increased to 2.77 in the sample collected after 72 min of treatment, reaching the maximum value of 16.66 in the sample at 120 min, after that the index decreased rapidly. The TU values estimated for each sample

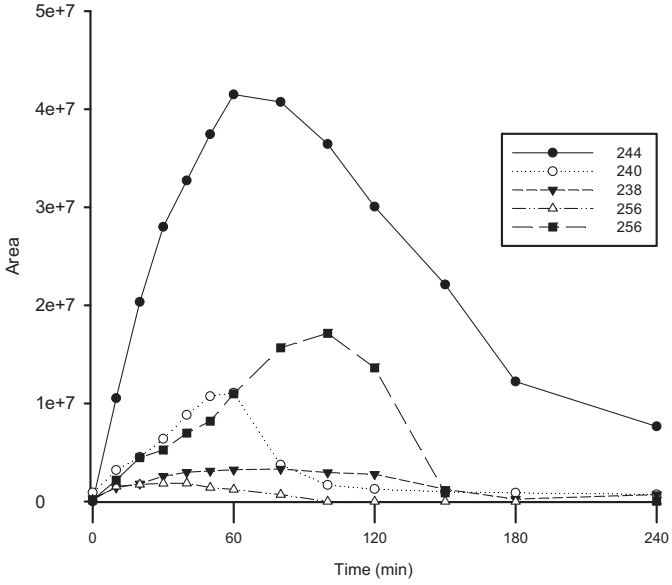

Fig. 13. Formation and degradation curves of main photoproducts obtained by using O_3/Hg-UV process and identified in the inset as nominal m/z ratios.

indicate that the tested solution belong to Class III (toxic), except for the sample collected after 120 min of treatment that pertains to Class IV (very toxic). From these results we can speculate that the treatment with O_3 under Hg-UV irradiation, implies the generation of some compounds more toxic than the parent substance, but this method is able to detoxify rapidly the effluent with the complete elimination of the more toxic intermediates. Fig. 13 shows the evolution of the major photoproducts obtained during the O_3/Hg-UV treatment. Similar results were shown also by O_3 and TiO_2/Xe-arc treatments.

In order to completely clarify such an evolution of toxicity, further systematic study on certain transformation product will be necessary, but this is not the aim of the present work.

4. Conclusion

The rate of mepanipyrim decomposition was highly dependent on the method used. Advanced oxidation processes, such as O_3, O_3/Hg-UV and TiO_2/Xe-arc, lead to a rapid decrease of the concentration of the biorecalcitrant pesticide in aqueous solutions, while Hg-UV, Xe-arc and Xe-arc/Pilkington Active™ Blue are less effective. The more effective degradation processes follow pseudo-first order kinetics, and the best results of pesticide degradation were obtained when O_3/Hg-UV system was applied. Noteworthy,

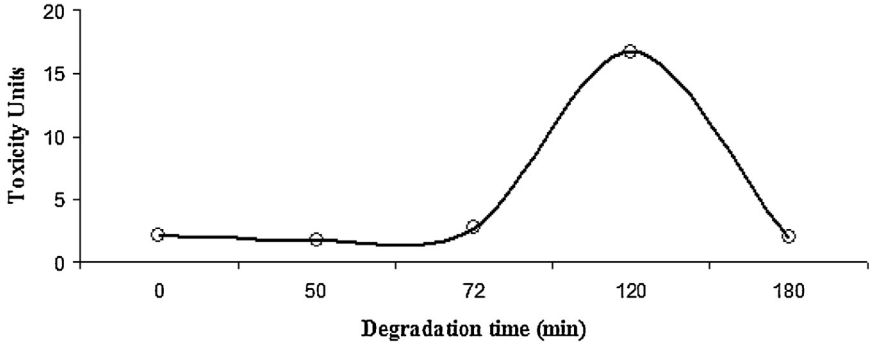

Fig. 12. Toxicity evolution of O_3/Hg-UV products using *V. fischeri* bioassay and initial mepanipyrim concentration of 22 mg L^{-1}.

no one of the methods tested has shown an AS degradation that can be described by a second-order reaction. Therefore, it can be concluded that the degradation rate was affected, at the most, by the variation of the remaining concentration of the reactant during the observation time, as in the case of first-order reactions. Absorption phenomena, when occurring, were never factors affecting the degradation rate.

Based on findings of this investigation, it is important to bear in mind that, when using the photocatalytic processes mediated by TiO_2 or O_3, the formation of transient organic compounds, some of them more toxic than the mother molecules, can occur. However, toxicity studies on the degraded mepanipyrim solutions showed that at the end of the photodegradation processes, intermediates were degraded too, giving a less toxic effluent. Fragments produced during CID analysis of the intermediates mentioned above are the diagnostic features of these compounds, which were used to identify them. Results of accurate mass measurements are another diagnostic feature of these compounds and proved to be useful to differentiate fragment with the same nominal mass but dissimilar exact masses

Due to a limited efficiency in the mepanipyrim degradation, the Xe-arc/Pilkington Active™ Blue system seems to be not useful for the scope, but by a practical point of view, it can be a promising system for removal recalcitrant compounds from wastewater not requiring the removal of the catalyst after the photo-degradation process. Further effort are needed for the preparation of TiO_2 coated materials, which could show a major efficiency in the photodegradation of recalcitrant substances.

Acknowledgements

This work was realized in the framework of the Project “Diffusion of nanotechnology based devices for water treatment and recycling—NANOWAT (1-B/2.1/049, Grant No.7/1997)", with the financial assistance of European Union under the ENPI-CBC-MED Program.

Appendix A. Supplementary data

Supplementary data associated with this article can be found, in the online version, at http://dx.doi.org/10.1016/j.jphotochem.2016.01.024.

References

[1] US Fish and Wildlife Service, Department of Environmental Quality. 2001. Pesticides and Wildlife. http://www.fws.gov/contaminants/Issues/Pesticides.cfm.
[2] C. Özdemir, S. Sahinkaya, M. Onüçyildiz, Asian J. Chem. 20 (2008) 3795–3804.
[3] U.S. EPA, Office of Pesticide Programs. “What is a Pesticide?” 2002. http://www.epa.gov/pesticides/about/.
[4] T. Heberer, J. Hydrol. 266 (2002) 175–189.
[5] T. Heberer, Toxicol. Lett. 131 (2002) 5–17.
[6] W. Glaze, J. Kang, D. Chapin, Ozone Sci. Eng. 9 (1987) 335–342.
[7] R. Munter, Proc. Est. Acad. Sci. Chem. 50 (2001) 59–80.
[8] V. Puddu, H. Choi, D.D. Dionysiou, G. Li Puma, Appl. Catal. B: Environ. 94 (2010) 211–218.
[9] O. Debono, F. Thevenet, P. Grevejat, V. Hequet, C. Raillard, L. Lecoq, N. Lecoge, Appl. Catal. B: Environ. 106 (2011) 600–608.
[10] M. Bekbölet, Water Sci. Technol. 35 (11–12) (1997) 95–100.
[11] N. Lydakis-Simantiris, D. Riga, E. Katsivela, D. Mantzavinos, N.P. Xekoukoulotakis, Desalination 250 (2010) 351–355.
[12] M. Kacem, G. Plantard, N. Wery, V. Goetz, Chin. J. Catal. 35 (2014) 1571–1577.
[13] P. Gorska, A. Zaleska, E. Kowalska, T. Klimczuk, J.W. Sobczak, E. Skwarek, W. Janusz, J. Hupka, Appl. Catal. B: Environ. 84 (2008) 440–447.
[14] A.H. Fostier, M.S.S. Pereira, S. Rath, J.R. Guimarães, Chemosphere 72 (2008) 319–324.
[15] G. Plantard, F. Correia, V. Goetz, J. Photochem. Photobiol. A: Chem. 222 (2011) 111–116.
[16] G. Plantard, V. Goetz, D. Sacco, Mater. Res. Bull. 46 (2011) 231–234.
[17] K. Elatmani, G. Plantard, D. Sacco, I. Aitichou, V. Goetz, Mater. Sci. Semicond. Process. 16 (2013) 1117–1124.
[18] J. Wiener, S. Shahidi, M.M. Goba, Opt. Laser Technol. 45 (2013) 147–153.
[19] L. Anfossi, P. Sales, A. Vanni, Pest. Manag. Sci. 62 (9) (2006) 872–879.
[20] M. Terada, F. Mizuhashi, K. Murata, T. Tomita, Toxicol. Appl. Pharmacol. 154 (1999) 1–11.
[21] P. Calza, C. Medana, C. Baiocchi, E. Pelizzetti, Int. J. Environ. Anal. Chem. 86 (3–4) (2006) 265–275.
[22] J. Kreuger, S. Graaf, J. Patring, S. Adielsson, Pesticides in surface water in areas with open ground and greenhouse horticultural crops in Sweden 2008, Uppsala 2010, ISSN 0347-9307
[23] J.C. D'Oliveira, C. Minero, E. Pelizzetti, P. Pichat, J. Photochem. Photobiol. A: Chem. 72 (1993) 261–267.
[24] Y. Ku, C.B. Hsieh, Water Res. 26 (11) (1992) 1451–1456.
[25] R.W. Matthews, Water Res. 24 (1990) 653–660.
[26] P. Calza, C. Medana, C. Baiocchi, P. Branca, E. Pelizzetti, J. Chromat. A 1049 (2004) 115–125.
[27] D.W. Sheel, R.J. McCurdy, S.J. Hurst, Patent application WO 98/06675.
[28] Pesticide Properties DataBase (PPDB), UK, University of Hertfordshire, 2016. (accessed 29.07.15) http://sitem.herts.ac.uk/aeru/ppdb/en/Reports/435htm.
[29] S.L. Murov, I. Carmichael, G.L. Hug, Handbook of Photochemistry, Marcel Dekker, Inc., New York, 1993, pp. 82–99.
[30] D.H. Volman, J.R. Seed, J. Am. Chem. Soc. 86 (23) (1964) 5095–5098.
[31] I. Stathis, D.G. Hela, L. Scrano, F. Lelario, L. Emanuele, S.A. Bufo, J, Environ. Sci. Health B 46 (6) (2011) 449–453.
[32] ISO, Water Quality: Determination of the Inhibitory Effect of Water Samples on the Light Emission of *Vibrio fischeri* (Luminescent Bacteria Test), ISO 11348-1, 2 and 3, International Standardization Organization, Geneva, Switzerland, 1998.
[33] Azur Environmental Ltd., Microtox® acute toxicity basic test procedures. Carlsbad, CA, USA, 1998.
[34] L. Scrano, S.A. Bufo, P. Perucci, P. Meallier, M. Mansour, Pestic. Sci. 55 (9) (1999) 955–961.
[35] S. Sulaiman, M. Khamis, S. Nir, F. Lelario, L. Scrano, S.A. Bufa, Environ. Technol. 35 (15) (2014) 1945–1955.
[36] L. Scrano, S.A. Bufo, M. D'Auria, C. Emmelin, J. Photochem. Photobiol. A: Chem. 129 (1–2) (1999) 65–70.
[37] L. Scrano, S.A. Bufo, M. D'Auria, P. Meallier, A. Behechti, K.W. Schramm, J. Environ. Qual. 31 (1) (2002) 268–274.
[38] E. Vulliet, C. Emmelin, L. Scrano, S.A. Bufo, J.M. Chovelon, P. Meallier, M.F. Grenier-Loustalot, J. Agric. Food Chem. 49 (10) (2001) 4795–4800.
[39] G.W. Snedecor, W.G. Cochran, Statistical Methods, 8th ed., Iowa State Univ. Press, Ames, 1989.
[40] R.H. Petrucci, W.S. Harwood, G. Herring, J.D. Madura, General Chemistry: Principles & Modern Applications, Ninth ed., Pearson Education, Upper Saddle River, N.J, 2007.
[41] F. Mendez-Arriaga, S. Esplugas, J. Gimenez, Water Res. 42 (2008) 585–594.
[42] A.P. Toor, A. Verma, C.K. Jotshi, P.K. Bajpai, V. Singh, Dyes Pigm. 68 (2006) 53–60.
[43] M. Brienza, M. Mahdi Ahmed, A. Escande, G. Plantard, L. Scrano, S. Chiron, S.A. Bufo, V. Goetz, Chem. Eng. J. 257 (2014) 191–199.
[44] M. Mahdi Ahmed, M. Brienza, V. Goetz, S. Chiron, Chemosphere 117 (2014) 256–261.
[45] A. Agüera, E. Almansa, A. Tejedor, A.R. Fernandez-Alba, S. Malato, M.I. Maldonado, Environ. Sci. Technol. 34 (8) (2000) 1563–1571.
[46] C. Sirtori, A. Zapata, S. Malato, A. Agüera, J. Hazard. Mater. 217 (2012) 217–223.
[47] G. Persoone, B. Marsalek, I. Blinova, A. Torkokne, D. Zarina, L. Manusadzianas, G. Nalecz-Jawecki, L. Tofan, N. Stepanova, L. Tothova, B. Kolar, Environ. Toxicol. 18 (2003) 395–402.